Synthesis via direct (hetero)arylation polymerization, electrochemical and optical properties of poly (3,4-disubstituted)thiophenes

Jérémie Grolleau, Stéphanie Legoupy, Pierre Frère, Frédéric Gohier

Synthesis via direct (hetero)arylation polymerization, electrochemical and optical properties of poly (3,4-disubtituted)thiophenes

Jérémie Grolleau, Stéphanie Legoupy, Pierre Frère* and Frédéric Gohier*

MOLTECH-Anjou, UMR 6200, CNRS, UNIV Angers, SFR MATRIX, 2 bd Lavoisier, 49045 ANGERS Cedex, France

email : pierre.frere@univ-angers.fr; frederic.gohier@univ-angers.fr

Abstract

Some poly (3,4-disubtituted)thiophenes bearing both cyano and alkoxy or thioalkoxy groups have been synthesized by direct (hetero)arylation polymerization (DHAP) of 2-iodo-3,4-disubstituted thiophenes. The electron donor and acceptor properties of substituents in positions 3 and 4 allow to adjust the HOMO and LUMO levels. On the other hand, in order to avoid the polymer solubility problems, long branched or unbranched alkyl chains have also been introduced. Thus polymers with alkoxy groups have led to complete absorption in the wavelength range of the visible spectrum whereas in the presence of thioalkoxy groups, the absorption of the visible spectrum is only partial. Theoretical calculations have shown that sulphur creates torsions leading to a non-planar polymer chain.

Key words: polythiophenes, direct heteroarylation polymerization, electronic properties

1-Introduction

Thiophene is a building block that will be found in many materials for optoelectronic applications. Polythiophenes are easily obtained, for example by Grignard Metathesis Polymerizations (GRIM), [1] Pd-catalyzed cross-coupling polycondensation[2] or more recently by direct arylation polymerization [3]which simply involves a C-H bond and a C-halogen bond so that the reaction can take place. There are a large number of papers describing polymers and copolymers based on thiophene using this methodology and a recent review by Pr Leclerc includes a number of examples.[4] P3HT, which has long remained the reference polymer as donor in organic photovoltaic cells [5], has been synthesized from bromo derivatives using Pd/NHC precursors, ligand and pivalic acid. [6] It can be synthesized in a simpler way, using Pd/C in phosphine free conditions. [7] Study on such type of polymers seems to be a way to explore to improve its properties for photovoltaic applications.

The energy levels of the HOMO and LUMO orbitals and therefore the bandwidth of the conjugated polymers can be controlled by the insertion of electron donor (D) and electron acceptor (A) units based on 3 and 4-substituted thiophenes. The electronic properties of conjugated polymers are highly dependent on the distribution of groups D and A along the conjugated skeleton. Introduction of cyano group into P3HT [8] affects the optoelectronic properties. The conjugation length is reduced which leads to an increase in the band gap. If an alkoxy chain replaces the hexyl chain in P3HT, the absorbance window is larger and the band gap is lowered. [9] Polymers carrying a cyanothiophene unit alternating or randomly with an alkylthiophene [10] as well as alkoxythiophene unit, [11] have already been reported so far. These materials result suitable optoelectronic properties in photovoltaic applications. Recently, we have synthesized thiophenes with an alkoxy group and cyano group.[12] We have shown that thiophene containing cyano and hexyloxy groups has electrochemical properties comparable to thiophene containing only the cyano group. However, optical properties were different. In this paper, we present the results of this same unit but within homopolymers. We also studied the effect of S in thioalkoxy chain instead of alkoxy chain on the properties of polymers.

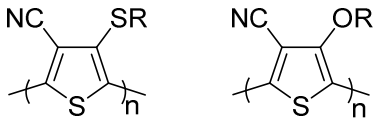

Figure 1

2-Experimental

2.1. Materials

NMR spectra were recorded on a Bruker Avance 300 (^{1}H: 300.1 MHz, ^{13}C: 75.7 MHz, T = 300 K). Spectra were referenced against the internal NMR-solvent standard. Chemical shifts were expressed in parts per million (ppm) and were reported as s (singlet), d (doublet), t (triplet), m (multiplet) and coupling constants *J* were given in Hz. Mass spectra were recorded under EI mode on a VG-Autospec mass spectrometer. The main peaks are described according to m/z. The peak corresponding to molecular mass is expressed as ($M^{+\bullet}$). Analytical grade solvents were used. Molecular weight analyses were performed on a Viscotek apparatus, composed of a GPC Max (comprising a degasser, a pump and an autosampler) with RI refractive index detector using a calibration with PS (sample from 1500g/mol to 1 500 000 g/mol with IP close to 1). THF was used as the eluent with a flow rate of 1.0 ml.min^{-1} at 30 °C. UV-Vis absorption spectra were recorded at room temperature on a Perkin Elmer Lambda 950 spectrometer and a PTI spectrofluorimeter mod. Quanta Master 1 coupled with a thermostat, using a Xenon lamp (70 W) as source and slits of 1 nm in a conventional quartz cell (light pass 10 mm). TGA analyses were performed with TA Instruments Q500. DSC analyses were performed with TA Instruments Q20. Cyclic voltammetry was performed using a Biologic SP-150 potentiostat with positive feedback compensation in dichloromethane solutions purchased from Carlo Erba (HPLC grade). Tetrabutylammonium hexafluorophosphate (0.1 M as supporting electrolyte) was purchased from Sigma-Aldrich. Experiments were carried out in a one-compartment cell equipped with platinum working microelectrode (Ø = 2 mm) and a platinum wire counter electrode. An $Ag/AgNO_3$ (0.01 M in CH_3CN) electrode was used as reference and checked against the ferrocene/ferricinium couple (Fc+/Fc) before and after each experiment. Theoretical calculations were done using the density functional theory with the Gaussian 09 program. The geometric optimization is based on the B3LYP hybrid functional with the 6-31G base (d, p).

2.2. Synthesis

The compounds **1**, [13] 2a and 3a [14] were synthesized from experimental data in the literature.

2.2.1. Synthesis of 4-(octadecyloxy)-2,5-dihydrothiophene-3-carbonitrile **2b**

To a solution of 4-oxotetrahydrothiophene-3-carbonitrile (1.02 g, 8.05 mmol) in dimethylformamide (10 mL), cesium carbonate (3.47 g, 10.65 mmol, 1.3 eq) and octadecyl methanesulfonate (3.56 g, 10.21 mmol, 1.3 eq) were added. The mixture was irradiated in CEM microwave open vessel (P:200 W, T:130°C) for 5 min. The mixture was poured into water, neutralized with diluted HCl (2M) and extracted with EtOAc (2 times). The organic layer was washed with saturated solution of NaCl, then water and dried over $MgSO_4$. The solvent was evaporated and the crude was purified through silica gel (petroleum ether/methylene chloride 1/1) to give a white solid (1.85g, 61%). mp 48-50°C. ^{1}H NMR (300 MHz, $CDCl_3$, ppm): δ 4.31 (t, 2H, J=6.6 Hz), 3.76 (s, 4H), 1.77-1.65 (m, 2H), 1.44-1.18 (m, 30H), 0.92-0.84 (m, 3H). ^{13}C NMR (77.16 MHz, $CDCl_3$, ppm): δ 169.1, 115.9, 80.7, 72.5, 36.2, 34.3, 32.0, 29.8, 29.7, 29.6, 29.5, 29.3, 25.7, 22.8, 14.2. HRMS (EI) calcd for $C_{23}H_{41}NOS$ [M+]: 379.2909, found: 379.2905.

2.2.2. Synthesis of 4-(decyloxy)-2,5-dihydrothiophene-3-carbonitrile **2c**

To a solution of 4-oxotetrahydrothiophene-3-carbonitrile (1.01 g, 7.94 mmol) in dimethylformamide (10 mL), cesium carbonate (3.1 g, 9.51 mmol, 1.2 eq) and 3,7-dimethyloctyl methanesulfonate (2.42 g, 10.24 mmol, 1.3 eq) were added. The mixture was irradiated in CEM microwave open vessel (P: 200 W, T:130°C) for 5 min. The mixture was poured into water, neutralized with diluted HCl (2M) and extracted with EtOAc (2 times). The organic layer was washed with saturated solution of NaCl, then water and dried over $MgSO_4$. The solvent was evaporated and the crude was purified through silica gel (petroleum ether/methylene chloride 1/1) to give a plate yellow oil (1.06g, 50%). ^{1}H NMR (300 MHz, $CDCl_3$, ppm): δ 4.42-4.27 (m, 2H), 3.76 (s, 4H), 1.81-1.68 (m, 1H), 1.65-1.45 (m, 3H), 1.34-1.09 (m, 6H), 0.91 (d, 3H, J=6.4 Hz), 0.86 (d, 6H, J=6.6 Hz). ^{13}C NMR (77.16 MHz, $CDCl_3$, ppm): δ 169.1, 115.9, 80.7, 70.9, 39.3, 37.2, 36.4, 36.3, 34.3, 29.6, 28.1, 24.7, 22.8, 22.7, 19.6. HRMS (EI) calcd for $C_{15}H_{25}NOS$ [M+]: 267.1657, found: 267.1660.

3.3.3 4-(octadecyloxy)thiophene-3-carbonitrile **3b**

To a solution of 4-(octadecyloxy)-2,5-dihydrothiophene-3-carbonitrile (1g, 2.63 mmol) in methylene chloride (30 mL) was stirred at 50°C then a solution of 2,3-dichloro-5,6-dicyano-1,4-benzoquinone (720 mg, 3.17 mmol, 1.2 eq) in THF (8 mL) was slowly added dropwise, and the mixture was stirred overnight at 50°C. After addition of water, the mixture was extracted with methylene chloride. The organic layer was dried over $MgSO_4$ and the solvent was removed under vacuum. The resulting crude product was purified over silica gel to give a white solid (655 mg, 66%). mp 75-77°C. ^{1}H NMR (300 MHz, $CDCl_3$, ppm): δ 7.76 (d, 1H, J=3.3 Hz), 6.26 (d, 1H, J=3.3 Hz), 3.99 (t, 2H, J=6.5 Hz), 1.87-1.76 (m, 2H), 1.50-1.21 (m, 30H), 0.90-0.85 (m, 3H). ^{13}C NMR ^{13}C NMR (77.16 MHz, $CDCl_3$, ppm): δ 157.7, 134.1, 113.5, 104.2, 98.0, 71.4, 32.0, 29.8, 29.7, 29.6, 29.5, 29.4, 29.0, 26.0, 22.8, 14.2. HRMS (EI) calcd for $C_{23}H_{39}NOS$ [M+]: 377.2752, found: 377.2747.

3.3.4 4-(decyloxy)thiophene-3-carbonitrile **3c**

To a solution of 4-(decyloxy)-2,5-dihydrothiophene-3-carbonitrile (800 mg, 3.01 mmol) in methylene chloride (30 mL) was stirred at 50°C then a solution of 2,3-dichloro-5,6-dicyano-1,4-benzoquinone (815 mg, 3.59 mmol, 1.2 eq) in THF (8 mL) was slowly added dropwise, and the mixture was stirred overnight at 50°C. After addition of water, the mixture was extracted with methylene chloride. The organic layer was dried over $MgSO_4$ and the solvent was removed under vacuum. The resulting crude product was purified over silica gel to give a colorless oil (718 mg, 90%). ^{1}H NMR (300 MHz, $CDCl_3$, ppm): δ 7.76 (d, 1H, J=3.3 Hz), 6.27 (d, 1H, 3.3 Hz), 4.07-4.00 (m, 2H), 1.92-1.80 (m, 1H), 1.71-1.46 (m, 3H), 1.36-1.10 (m, 6H), 0.94 (d, 3H, J=6.4 Hz), 0.87 (d, 6H, J=6.6 Hz). ^{13}C NMR (77.16 MHz, $CDCl_3$, ppm): δ 157.7, 134.2, 113.5, 104.2, 98.0, 69.8, 39.3, 37.3, 35.9, 29.9, 28.1, 24.7, 22.8, 22.7, 19.7. HRMS (EI) calcd for $C_{15}H_{23}NOS$ [M+]: 265.1500, found: 265.1494.

3.3.5 4-(hexylthio)thiophene-3-carbonitrile **6a**

A solution of 4-bromothiophene-3-carbonitrile (465 mg, 2.47 mmol), tributyl(hexylthio)stannane (2.05 g, 5.03 mmol, 2 eq), and $Pd(PPh_3)_4$ (850 mg, 0.74 mmol, 30% mol) in dry toluene (25 mL) was heated at 120°C for 12 h. The organic layer was diluted with EtOAc and washed with an aqueous solution of $NaHCO_3$, then water, dried over $MgSO_4$ and the solvent was removed under vacuum. The crude was purified over silica gel (methylene chloride/petroleum ether 6/4) to give a yellow oil (507 mg, 91%). ^{1}H NMR (300 MHz, $CDCl_3$, ppm): δ 7.95 (d, 1H, J=3.2 Hz), 7.22 (d, 1H, J=3.2 Hz), 2.91 (t, 2H, J=7.4 Hz), 1.67-1.57 (m, 2H), 1.46-1.36 (m, 2H), 1.31-1.25 (m, 4H), 0.88 (t, 3H, 6.8 Hz). ^{13}C NMR (77.16 MHz, $CDCl_3$, ppm): δ 136.5, 135.1, 125.7, 114.6, 114.2, 35.5, 31.4, 29.6, 28.4, 22.6, 14.1. HRMS (CI) calcd for $C_{11}H_{15}NS_2$ [M+]: 225.0646, found: 225.0647.

3.3.6 4-(octadecylthio)thiophene-3-carbonitrile **6b**

A solution of 4-bromothiophene-3-carbonitrile (502 mg, 2.67 mmol), tributyl(hexylthio)stannane (3.2 g, 5.56 mmol, 2 eq), and $Pd(PPh_3)_4$ (932 mg, 0.81 mmol, 30% mol) in dry toluene (15 mL) was heated at 120°C for 12 h. The organic layer was diluted with EtOAc and washed with an aqueous solution of $NaHCO_3$, then water, dried over $MgSO_4$ and the solvent was removed under vacuum. The crude was purified over silica gel (methylene chloride/petroleum ether 6/4) to give a plate yellow solid (771 mg, 73%). mp 57-59°C. ^{1}H NMR (300 MHz, $CDCl_3$, ppm): δ 7.95 (d, 1H, J=3.2Hz), 7.22 (d, 1H, J=3.2 Hz), 2.91 (t, 2H, J=7.4 Hz), 1.68-1.55 (m, 2H), 1.46-

1.19 (m, 30H), 0.91-0.83 (m, 3H). ^{13}C NMR (77.16 MHz, $CDCl_3$, ppm): δ 136.4, 135.0, 125.5, 114.5, 114.1, 35.4, 32.0, 29.8, 29.7, 29.6, 29.5, 29.2, 28.7, 22.8, 14.2. HRMS (EI) calcd for $C_{23}H_{39}NS_2$ [M+]: 393.2524, found: 393.2517.

3.3.7 4-(hexyloxy)-5-iodothiophene-3-carbonitrile **4a**

4-(hexyloxy)thiophene-3-carbonitrile (202 mg, 0.97 mmol) was dissolved in EtOH (8 mL) at 50°C. Then, NIS (452 mg, 2 mmol, 2.1 eq) was added followed by PTSA (18mg, 0.1 mmol, 10%mol). The mixture was stirred 10 min, then saturated $Na_2S_2O_3$ (2 mL) was added. The mixture was diluted with EtOAc. After organic layer was washed with 1M Na_2CO_3 solution, dried over $MgSO_4$, filtered, and evaporated to give a yellow oil (320 mg, 98%). ^{1}H NMR (300 MHz, $CDCl_3$, ppm): δ 7.96 (s, 1H), 4.20 (t, 2H, J=6.5 Hz), 1.85-1.75 (m, 2H), 1.57-1.46 (m, 2H), 1.39-1.31 (m, 4H), 0.91 (t, 3H, J=7.0 Hz). ^{13}C NMR (77.16 MHz, $CDCl_3$, ppm): δ 159.2, 139.4, 112.8, 105.9, 75.4, 62.2, 31.6, 30.0, 25.6, 22.7, 14.2. HRMS (EI) calcd for $C_{11}H_{14}INOS$ [M+]: 334.9841, found: 334.9831.

3.3.7 5-iodo-4-(octadecyloxy)thiophene-3-carbonitrile **4b**

4-(octadecyloxy)thiophene-3-carbonitrile (200.5 mg, 0.54 mmol) was dissolved in EtOH (4 mL) at 50°C. Then, NIS (252 mg, 1.12 mmol, 2.1 eq) was added followed by PTSA (11mg, 0.06 mmol, 10%mol). The mixture was stirred 10 min, then saturated $Na_2S_2O_3$ (2 mL) was added. The mixture was diluted with EtOAc. After organic layer was washed with 1M Na_2CO_3 solution, dried over $MgSO_4$, filtered, and evaporated to give a yellow oil (270 mg, 99%). ^{1}H NMR (300 MHz, $CDCl_3$, ppm): δ 7.96 (s, 1H), 4.20 (t, 2H, J=6.5 Hz), 1.85-1.75 (m, 2H), 1.55-1.20 (m, 30H), 0.91-0.85 (m, 3H). ^{13}C NMR (77.16 MHz, $CDCl_3$, ppm): δ 159.1, 139.3, 112.7, 105.8, 75.4, 62.2, 32.0, 30.0, 29.8, 29.7, 29.5, 29.4, 25.9, 22.8, 14.2. HRMS (EI) calcd for $C_{23}H_{38}INOS$ [M+]: 503.1719, found: 503.1720.

3.3.8 4-(decyloxy)-5-iodothiophene-3-carbonitrile **4c**

4-(decyloxy)thiophene-3-carbonitrile (311 mg, 1.17 mmol) was dissolved in EtOH (6 mL) at 50°C. Then, NIS (514 mg, 2.28 mmol, 2 eq) was added followed by PTSA (20 mg, 0.12 mmol, 10%mol). The mixture was stirred 10 min, then saturated $Na_2S_2O_3$ (3 mL) was added. The mixture was diluted with EtOAc. After organic layer was washed with 1M Na_2CO_3 solution, dried over $MgSO_4$, filtered, and evaporated to give a yellow oil (411 mg, 90%). ^{1}H NMR (300 MHz, $CDCl_3$, ppm): δ 7.96 (s, 1H), 4.31-4.18 (m, 2H), 1.92-1.80 (m, 1H), 1.79-1.67 (m, 1H), 1.66-1.46 (m, 2H), 1.38-1.11 (m, 6H), 0.96 (d, 3H, J=6.5 Hz), 0.87 (d, 6H, J=6.6 Hz). ^{13}C NMR (77.16 MHz, $CDCl_3$, ppm): δ 159.2, 139.4, 112.7, 105.8, 73.8, 62.2, 39.4, 37.3, 37.1, 29.6, 28.1, 24.8, 22.8, 22.7, 19.7. HRMS (EI) calcd for $C_{15}H_{22}INOS$ [M+]: 391.0467, found: 391.0457.

3.3.9 4-(hexylthio)-5-iodothiophene-3-carbonitrile **7a**

4-(hexylthio)thiophene-3-carbonitrile (100.5 mg, 0.45 mmol) was dissolved in EtOH (4 mL) at 50°C. Then, NIS (111 mg, 0.49 mmol, 1.1 eq) was added followed by PTSA (8mg, 0.048 mmol, 10%mol). The mixture was stirred 10 min, then saturated $Na_2S_2O_3$ (2 mL) was added. The mixture was diluted with EtOAc. After organic layer was washed with 1M Na_2CO_3 solution, dried over $MgSO_4$, filtered and evaporated to give a yellow oil (148 mg, 94%). ^{1}H NMR (300 MHz, $CDCl_3$, ppm): δ 8.07 (s, 1H), 2.89 (t, 2H, J=7.2 Hz), 1.6-1.49 (m, 2H), 1.47-1.37 (m, 2H), 1.32-1.23 (m, 4H), 0.87 (t, 3H, J=6.9 Hz). ^{13}C NMR (77.16 MHz, $CDCl_3$, ppm): δ 141.0, 139.9, 116.0, 113.7, 88.3, 36.4, 31.4, 29.7, 28.3, 22.6, 14.2. HRMS (EI) calcd for $C_{11}H_{14}INS_2$ [M+]: 350.9612, found: 350.9615

3.3.10 5-iodo-4-(octadecylthio)thiophene-3-carbonitrile **7b**

4-(octadecylthio)thiophene-3-carbonitrile (301 mg, 0.76 mmol) was dissolved in EtOH (6 mL) at 50°C. Then, NIS (344 mg, 1.53 mmol, 2 eq) was added followed by PTSA (18 mg, 0.1 mmol, 10%mol). The mixture was stirred 10 min, then saturated $Na_2S_2O_3$ (3 mL) was added. The mixture was diluted with EtOAc. After organic layer was washed with 1M Na_2CO_3 solution, dried over $MgSO_4$, filtered, and evaporated to give a white solid

(358 mg, 91%). mp: 81-83°C. ^{1}H NMR (300 MHz, $CDCl_3$, ppm): δ 8.07 (s, 1H), 2.88 (t, 2H, J=7.2 Hz), 1.61-1.49 (m, 2H), 1.45-1.21 (m, 30H), 0.91-0.84 (m, 3H). ^{13}C NMR (77.16 MHz, $CDCl_3$, ppm): δ 140.9, 139.9, 116.0, 113.6, 88.2, 36.3, 32.0, 29.8, 29.7, 29.6, 29.5, 29.2, 28.6, 22.8, 14.2. HRMS (EI) calcd for $C_{23}H_{38}INS_2$ [M+]: 519.1490, found: 519.1475.

3.3.11 General procedure for direct arylation polymerization:

A mixture of 4-(alkyl)-5-iodothiophene-3-carbonitrile (200 mg), potassium carbonate (3 eq) and palladium acetate (10% mol) was stirred in *N*-*N*-dimethylformamide (6 mL) for 40 h at 80°C under an argon atmosphere. An aqueous solution was added, and the precipitate was separated by filtration and washed with distilled water and methanol. The precipitate was filtered through a Soxhlet thimble and purified via Soxhlet extraction for 4 h with methanol then 20 h with hexane. The polymer was finally collected from chloroform, and the resulting solution was then concentrated by evaporation to give the desired polymers.

Poly-4-(octadecyloxy)thiophene-3-carbonitrile **Poly 4b**

Dark powder, 63 %. SEC: M_n (KDa)= 7.6, M_w (KDa)=16.1, PDI=2.1

Poly-4-(decyloxy)thiophene-3-carbonitrile **Poly 4c**

Dark powder, 69 %. SEC: M_n (KDa)= 7.5, M_w (KDa)=21.0, PDI=2.8

Poly-4-(octadecylthio)thiophene-3-carbonitrile **Poly 7b**

Dark powder, 36 %. SEC: M_n (KDa)= 1.8, M_w (KDa)=5.8, PDI=3.2

3. Results and discussion

Access to the various monomers was achieved by two synthesis methods. The first allows synthesis of compounds **4** from compound **1** and the second allows the introduction of thioalkoxy chain from brominated derivative **5** to lead to derivatives **7**. Compound **1** obtained by condensation of acrylonitrile with ethyl thioglycolate ester leads to derivatives **2** by alkylation of enolate following by aromatization to obtain the thiophene **3**. Attempts to obtain thioketone from ketone 1 via Lawesson's reagent failed. Thioalkyl chains were therefore introduced by Stille cross-coupling since the bromine-lithium exchange does not allow the functionalization of position 3 due to lithium dance in position 2. The iodination is then carried out with excellent yields without any purification according to a protocol we have reported. [15]

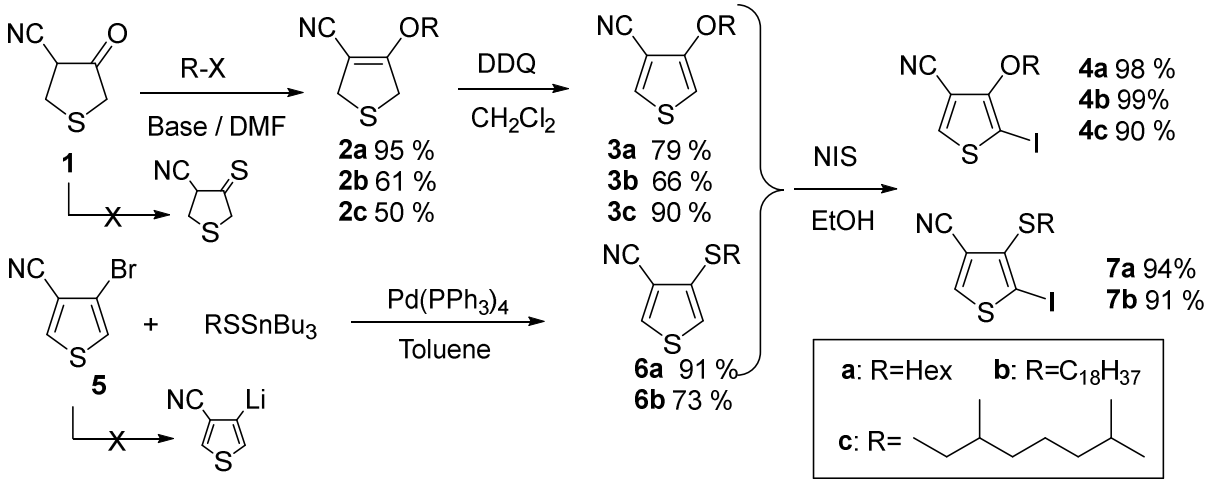

Scheme 1: Syntheses of thiophene monomers

The polymer synthesis was carried out according to a direct arylation polymerization.[3b] Simple conditions were used based on the work of Lemaire et al. [16] The polymerization of the various monomers was carried out at 80°C in DMF with $Pd(OAc)_2$ as catalyst and K_2CO_3. In Lemaire's procedure, they used Bu_4NBr, however, in our case, the results are identical with or without this co-reagent. The addition of the catalyst in the medium causes a colour change from red to black blue. The resultant polymers are purified by Soxhlet extraction with different solvents to remove unpolymerized organic compounds. Polymer **4a** with the hexyl chain could not be analyzed due to its insolubility in common organic solvent and monomer **7a** could not polymerize. When a C18 linear chain is present, the polymers are more soluble, however the yield for the thioalkyl polymer (**Poly 7b**) is modest (36%). Sulphur containing species are known to have poisoning effects on metal catalyst, which has been confirmed by direct arylation tests with monomer **6a**. Indeed, **6a** in presence of bromobenzene, catalyst, ligand and base could not be functionalized; such result explains the impossibility to obtain **poly 7a**. Polymerizations with alkoxys were obtained with good yields (63 and 69% for **4b** and **4c**), the polymers being quite soluble.

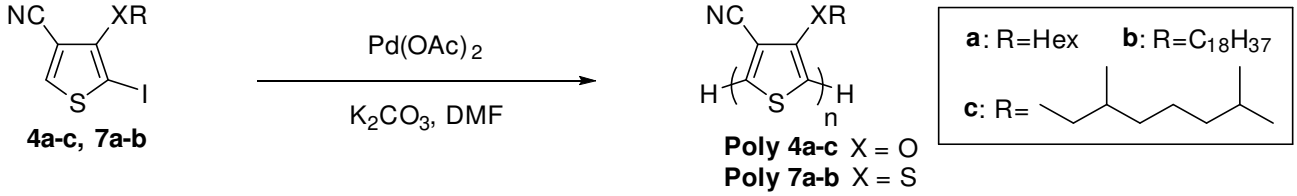

Scheme 2: Polymerization of thiophene monomers

Molecular weights were measured by SEC and indicate that polymers were obtained with quite short chains (around 9000 g/mol for **poly 4b** and **poly 4c**) and with a high polydispersity. Very short chains for the thioalkyl derivative (2000 g/mol) were detected in SEC confirming the difficulty to polymerize the thioalkyl derivative. The degradation temperatures of the various polymers were also determined by TGA and proved satisfactory for applications such as solar energy as materials begin to degrade around 280°C for **poly 4** (see SI). DSC analyses were also done on the different materials and showed transition glass between 50 °C and 70°C (see SI) for **poly 4a** and **poly 7b**.

Optical properties of the polymers were analyzed by UV-Visible spectroscopy in solution in chloroform (Figure 2a) and in thin film deposited on glass by spin-coating (Figure 2b).

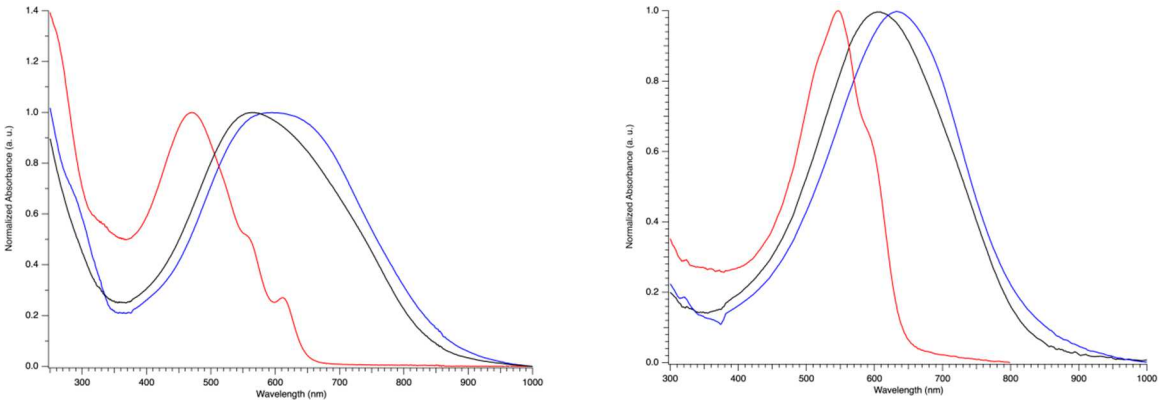

Figure 2: a) UV-Visible spectra of **poly 4b** (black), **poly 4c** (blue) and **poly 7b** (red) in $CHCl_3$. b) UV-Visible spectra of films on glass of **poly 4b** (black), **poly 4c** (blue) and **poly 7b** (red).

The **poly 4b** and **poly 4c** polymers have a wide absorption band centered at 565 and 605 nm respectively, covering the spectrum from 400 to 800 nm. The absorption band of the **poly 7b** at 472

nm has several shoulders that may be due to a mixture of oligomers, in accordance with the broad polydispersity observed in SEC. On film, displacements of about 40, 30 and 75 nm are observed for **poly 4a**, **poly 4b** and **poly 7b** respectively. The observed bathochromic displacement results from a reorganization of the polymer chains in the solid state and its skeleton (stacking). For **poly 7b**, this effect is more important, meaning an increase of conjugation in solid state. Our attention has been drawn to the hypsochromic displacement of **poly 7b** in comparison with **poly 4**. This can be explained by the larger sulfur atom creating an S---S repulsion then causing a conjugation breakdown.[17] In contrast, in **poly 4b** and **poly 4c**, S---O interactions are favourable and increase electron delocalization.[18] In order to check the influence of donor and acceptor groups on the same thiophene motif on electronic properties, theoretical calculations using the density functional theory of using the Gaussian 09 program were realized. The geometric optimization based on the B3LYP hybrid functional with the 6-31G base (d, p) was realized on bithiophene to sexithiophene. To reduce the calculation time, the alkyl chain is reduced to a propyl chain. Results are gathered in the table 1.

Table 1: HOMO/LUMO determination by geometric optimization of oligomers of 3-alkoxy/3-thioalkoxy-4-cyanothiophene

Oligomers	Chain	HOMO (eV)	LUMO (eV)	Gap (eV)	Average torsion angle (°)
Dimer	alcoxy	- 6.13	- 2.23	3 90	4
	thioether	- 6.37	- 2.24	4 13	45
Trimer	alcoxy	- 5.82	- 2.60	3.22	1
	thioether	- 6.36	- 2.55	3.81	45
Tétramer	alcoxy	- 5.67	-2.80	2.87	2
	thioether	- 6.34	- 2.71	3.63	43
Pentamer	alcoxy	- 5.51	- 2.88	2.63	2
	thioether	- 6.05	- 3.00	3.05	28
Hexamer	alcoxy	- 5.51	- 3.01	2.50	1
	thioether	- 5.94	- 3.15	2.79	19

For alkoxy derivatives, the geometric modeling of each oligomer leads to a flat structure with an S--O interaction. In the case of oligomers with the thioether chain, geometric modelling for dimer, trimer and tetramer predicts a non-planar molecule with a torsion between each thiophene due to a repulsion between sulphurs. In the cases of pentamer and hexamer, the modelling leads to a much flatter carbon skeleton, which leads to a significant decrease in the HOMO-LUMO energy gap compared to the previous cases. These data are very well illustrated by the theoretical representations of trimers and hexamers in which no torsion is visible with alkoxy side chain (figure 3a-b) while thioalkoxy side chain (figure 3c-d) causes skeletal torsion.

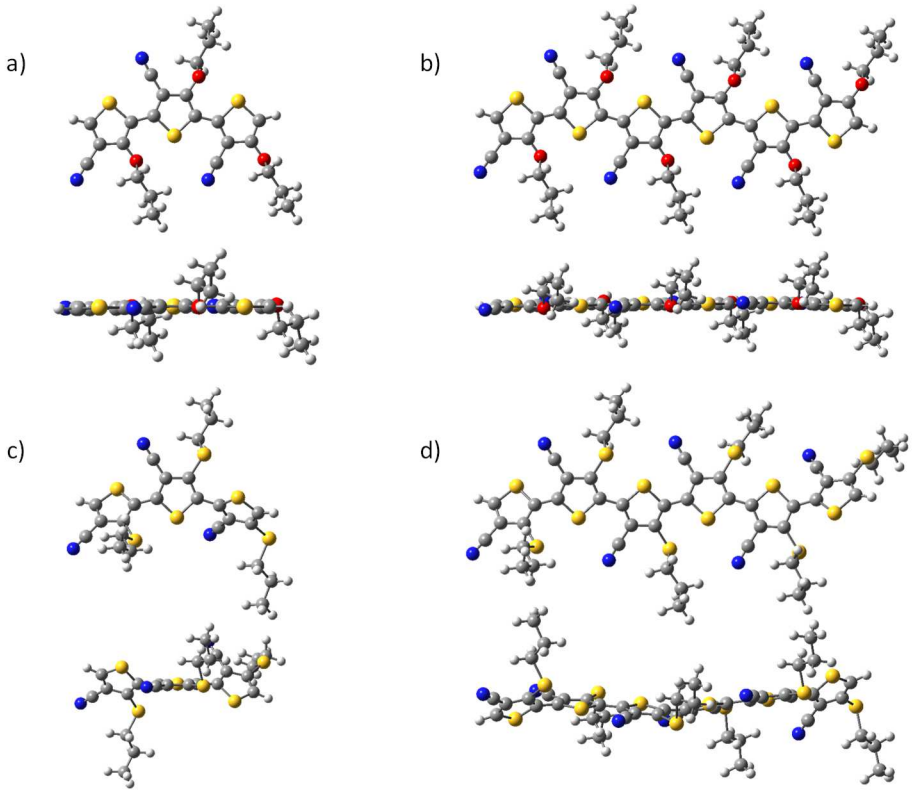

Figure 3: Theoretical structure of the trimer and hexamer with an alkoxy chain (a and b) and with a thioether chain (c and d).

The band gap energies were first estimated from UV absorption spectra by measuring the change in optical absorption. Band gaps extrapolated from the foot edge of the absorption bands are 1.50, 1.51 and 1.92 eV for **poly 4b**, **poly 4c** and **poly 7b** respectively. The band gap energies were also determined by electrochemistry and show results consistent with the optical gaps (see table 2). We also plotted ΔE as a function of 1/n (figure 4) to determine theoretical band gaps. We were able to estimate that the theoretical gap of poly(alkoxycyanothiophene) **4** was 1.80. The regression line for poly(thioalkoxycyanothiophenes) is less demonstrative due to the lower flatness of the small oligomers and the estimated ΔE is 2.38 eV. All these results are consistent with experimental data. The cyclic voltammograms of the **poly 4b** and **poly 4c** polymers are similar and have two reversible oxidation waves at 0.74 and 0.70 V respectively for the first wave and 1.34 V and 1.10 V for the second (table 2). The **poly 7b** polymer is irreversibly oxidizable at 1.42 V. In reduction, the **poly 4b** and **poly 4c** polymers have irreversible peaks at -1.45 and -1.39 V respectively, for **poly 7b** the reduction is almost reversible at -1.57 V. The **poly 4b** and **poly 4c** polymers which differ only with the alkyl chain have equivalent electrochemical properties. On the other hand, the substitution of oxygen by sulphur increases the oxidation and reduction potential by about 700 mV and 150 mV respectively. The more difficult oxidation of **poly 7b** can be explained by the more electron-donating thioether chain and by unfavorable S---S interactions that reduce conjugation. Considering the onset of oxidation and reduction waves, the HOMO and LUMO levels can be determined experimentally and are shown in Figure 5.

Table 2: Electrochemical results on polymers **poly 4b-4c-7b**

Compounds	E_{ox} [a] (V)	E_{red} [a] (V)	E_{HOMO} [b] (eV)	E_{LUMO} [b] (eV)	ΔE_{elec} (eV)	ΔE_{opt} (eV)[c]	ΔE_{th} (eV)[d]
Poly 4b	0.74 / 1.34	-1.45	-5.97	-4.13	1.84	1.50	1.80
Poly 4c	0.70 / 1.10	-1.39	-5.93	-4.12	1.81	1.51	1.80
Poly 7b	1.42	-1.57	-6.52	-4.09	2.43	1.92	2.38

[a] **poly 4b-c, poly 7b** deposited on the electrode in 0.1 M Bu_4NPF_6–CH_2Cl_2, v = 100 $mV.s^{-1}$, Pt electrode, ref. Fc/Fc^+. [b] Using an offset of -4.99 eV compared to SCE.[19]. [c] Band gaps extrapolated from the foot edge of the absorption bands. [d] Determined from fig 4 by extrapolation of plot $\Delta E = f(1/n)$.

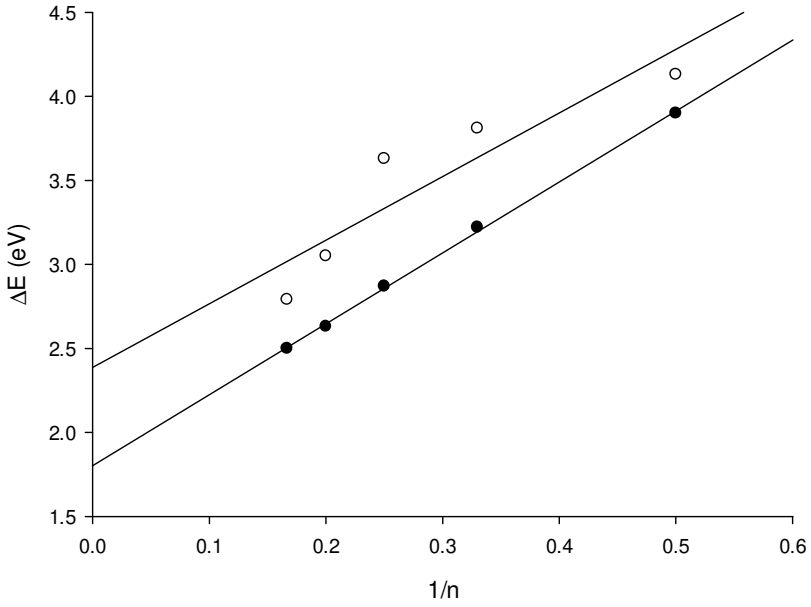

Figure 4: Band width evolution as a function of 1/n where n is the number of monomer in the molecule. Full circle: alkyloxycyanothiophene unit and empty circle: thioalkoxycyanothiophene unit

HOMO/LUMO levels are stabilized relative to P3HT showing the importance of thiophene substitution whatever the data we are taking into account.[20] Sulphur is much more stabilizing than oxygen and cyano has a comparable effect regardless of the polymers. These energy levels would be interesting to use these materials as acceptors rather than donors in solar energy conversion devices.

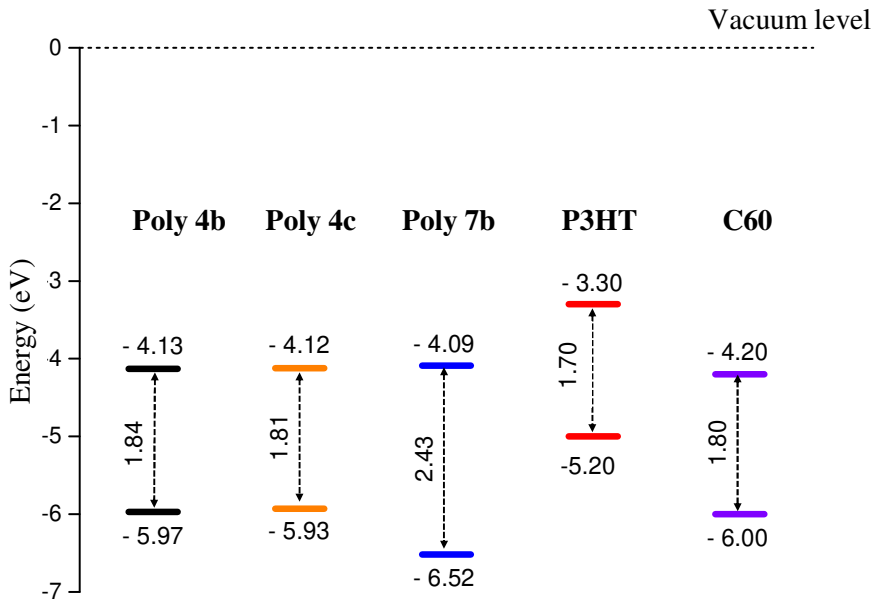

Figure 5: Experimental HOMO/LUMO levels of **Poly 4b**, **Poly 4c** and **Poly 7b** compared to P3HT.

4. Conclusion

In conclusion, several 3 and 4 substituted polythiophenes with donor and acceptor groups in these positions have been obtained. These groups will greatly influence the electrooptical properties of the final material since spectral coverage is very wide in the presence of an alkoxy group in position 3 whereas in the presence of thioalkoxy, this coverage is lower. The break-up of the conjugation seems to be responsible for this difference. On the other hand, HOMO/LUMO levels have been affected by these substitutions, and these levels are far from levels of the P3HT, thus attempts to use these materials as donors or acceptors will be considered in future works.

Acknowledgements

We thank the university of Angers for Jérémie Grolleau's grant.

References

[1] aR. D. McCullough, R. D. Lowe, *Journal of the Chemical Society, Chemical Communications* **1992**, 70-72; bR. Miyakoshi, A. Yokoyama, T. Yokozawa, *Journal of the American Chemical Society* **2005**, *127*, 17542-17547.

[2] aM. A. Baker, C.-H. Tsai, K. J. T. Noonan, *Chemistry – A European Journal* **2018**, *24*, 13078-13088; bin *Synthetic Methods for Conjugated Polymers and Carbon Materials*, pp. 59-95.

[3] a) D. Alberico, M. E. Scott, M. Lautens, *Chem Rev* **2007**, *107*, 174-238; b) M. Wakioka, F. Ozawa, *Asian Journal of Organic Chemistry* **2018**, *7*, 1206-1216; c) H. Bohra, M. Wang, *Journal of Materials Chemistry A* **2017**, *5*, 11550-11571.

[4] J. T. Blaskovits, M. Leclerc, *Macromol Rapid Comm* **2019**, *40*, 1800512.

[5] aQ. Pierluigi, F. Andrea, *Letters in Organic Chemistry* **2018**, *15*, 991-1006; bJ. Roncali, *Chem Rev* **1992**, *92*, 711-738.

[6] Y.-Y. Lai, T.-C. Tung, W.-W. Liang, Y.-J. Cheng, *Macromolecules* **2015**, *48*, 2978-2988.

[7] S. Hayashi, Y. Kojima, T. Koizumi, *Polymer Chemistry* **2015**, *6*, 881-885.

[8] C. L. Chochos, S. P. Economopoulos, V. Deimede, V. G. Gregoriou, M. T. Lloyd, G. G. Malliaras, J. K. Kallitsis, *The Journal of Physical Chemistry C* **2007**, *111*, 10732-10740.

[9] C. Shi, Y. Yao, Yang, Q. Pei, *Journal of the American Chemical Society* **2006**, *128*, 8980-8986.
[10] aA. E. Rudenko, P. P. Khlyabich, B. C. Thompson, *Acs Macro Lett* **2014**, *3*, 387-392; bA. E. Rudenko, P. P. Khlyabich, B. C. Thompson, *Journal of Polymer Science Part A: Polymer Chemistry* **2016**, *54*, 1526-1536.
[11] S. Berson, S. Cecioni, M. Billon, Y. Kervella, R. de Bettignies, S. Bailly, S. Guillerez, *Sol Energ Mat Sol C* **2010**, *94*, 699-708.
[12] J. Grolleau, F. Gohier, C. Cabanetos, M. Allain, S. Legoupy, P. Frère, in *Organic & biomolecular chemistry, Vol. 14*, Royal Society of Chemistry, Cambridge, **2016**, pp. 10516-10522.
[13] P. G. Baraldi, G. P. Pollini, V. Zanirato, A. Barco, S. Benetti, *Synthesis* **1985**, *1985*, 969-970.
[14] N. Hergué, C. Mallet, G. Savitha, M. Allain, P. Frère, J. Roncali, *Org Lett* **2011**, *13*, 1762-1765.
[15] J. Grolleau, P. Frère, F. Gohier, *Synthesis* **2015**, *47*, 3901-3906.
[16] M. Se´vignon, J. Papillon, E. Schulz, M. Lemaire, *Tetrahedron Letters* **1999**, *40*, 5873-5876.
[17] M. Turbiez, P. Frère, M. Allain, N. Gallego-Planas, J. Roncali, *Macromolecules* **2005**, *38*, 6806-6812.
[18] aJ. Roncali, P. Blanchard, P. Frère, *J Mater Chem* **2005**, *15*, 1589-1610; bG. Conboy, H. J. Spencer, E. Angioni, A. L. Kanibolotsky, N. J. Findlay, S. J. Coles, C. Wilson, M. B. Pitak, C. Risko, V. Coropceanu, J.-L. Brédas, P. J. Skabara, *Materials Horizons* **2016**, *3*, 333-339; cH. Huang, L. Yang, A. Facchetti, T. J. Marks, *Chem Rev* **2017**, *117*, 10291-10318.
[19] C. M. Cardona, W. Li, A. E. Kaifer, D. Stockdale, G. C. Bazan, *Adv Mater* **2011**, *23*, 2367-2371.
[20] aP. Acevedo-Peña, A. Baray-Calderón, H. Hu, I. González, V. M. Ugalde-Saldivar, *Journal of Solid State Electrochemistry* **2017**, *21*, 2407-2414; bS. Berson, R. de Bettignies, S. Bailly, S. Guillerez, B. Jousselme, *Advanced Functional Materials* **2007**, *17*, 3363-3370.

Submission of manuscript to Solar Energy

Photometrical analysis of Mirrored Light Pipe:

from state-of-the-art on experimental results (1990-2019) to the proposition of new experimental observations in high solar potential climates

---

Bruno MALET-DAMOUR, Dimitri BIGOT, Stéphane GUICHARD and Harry BOYER

Contents:

- *Revised Manuscript*

Corresponding author:

Bruno MALET-DAMOUR

Physics and Mathematical Engineering Laboratory for Energy, Environment and Building (PIMENT)

University of La Reunion,

117, rue du Général Ailleret

97430 Le Tampon (France)

tél : 06 92 81 95 96

fax : 02 62 96 28 59

email : bruno.malet-damour@univ-reunion.fr

Photometrical analysis of Mirrored Light Pipe:

from state-of-the-art on experimental results (1990-2019) to the proposition of new experimental observations in high solar potential climates

Bruno MALET-DAMOUR[1], Dimitri BIGOT, Stéphane GUICHARD and Harry BOYER

University of La Reunion, Physics and Mathematical Engineering Laboratory for Energy, Environment and Building (PIMENT)
117, rue du Général Ailleret 97 430 Le Tampon, France.
1 : Phone +262 (0) 692 81 95 96, Fax (+262) 96 28 59, email : bruno.malet-damour@univ-reunion.fr

Graphical abstract :

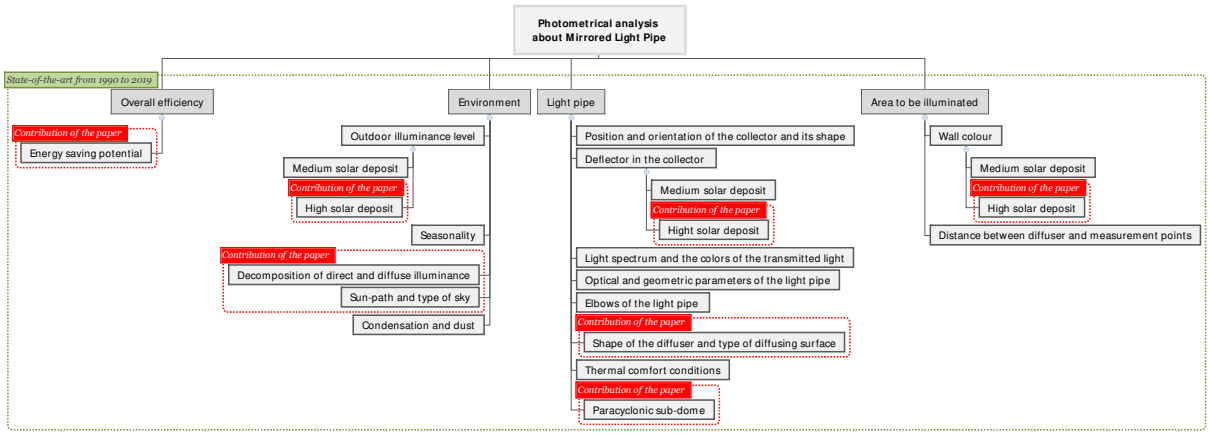

Abstract :

This paper focuses on the part of Tubular Daylight Guide Systems (TDGS): the Mirrored Light-Pipe (MLP). MLP is part of the multiple specular reflection conveyors. They allow daylight to be transported and distributed in dark rooms far from traditional openings while limiting heat transmission. It involves collecting, concentrating, and diffusing sunlight using a dome placed on the roof. It is then conveyed through a highly reflective tube and diffused into a building's room using a diffuser.

Previous work (Malet-Damour et al., 2017, 2016) has shown that it was necessary to identify and study the climate in which the light pipe will be installed. A state-of-the-art of experimental and numerical results was conducted over the period from1990 to 2019. It revealed that the behavior of the light pipe depends strongly on the indoor (area to be illuminated) and outdoor (meteorology) environment.

This paper presents the experimental observations of studies conducted from 2013 to 2015 on Mirrored Light-Pipe in Reunion Island. The climate in which the experiment was undertaken is presented with a focus on illuminance. In 2019, this study is the only one analyzing the performance of the light pipe in extreme situations of extreme sunlight conditions (maximum global illuminance of around 200 Klux). Experimental results based on various scenarios quantified the impact of the reflection coefficient of the area to be illuminated, the presence of an anticyclonic dome, the type of sky or the ideal position of a sub-dome deflector. The results are very encouraging.

Keywords: Mirrored Light Pipe; Experiment; Tubular Daylight Guide Systems; Review; Photometrical analysis; Daylight

Nomenclature

τ_{TDGS}	Transmission coefficient of the light pipe	[-]
ρ_{LP}	Internal reflectivity coefficient	[-]
ρ_{moy}	Average reflection coefficient of the walls test cell's	[-]
ρ_{PV}	Wall reflection coefficient	[-]
Ap	Aspect ratio, ratio between length L and diameter D of the light pipe	[-]
Ai	Reference of luxmeters position's inside the test cell	[-]
D	Euclidean distance (diffuser - point to illuminate)	[m]
DPF	Daylight Penetration Factor, ratio between indoor and outdoor illuminance	[-]
H	Vertical height of the diffuser	[m]
k_t	Brightness index	[-]

1. Introduction

Nowadays, due to climatic and energetic concerns, it is crucial to building sector to provide many solutions. The challenge is to limit the impact of buildings on energy consumption even more so greenhouse gas emissions which are responsible for global warming. That is why, it is essential to conduct investigations of passive lighting systems to use natural lighting as possible, to increase both visual and thermal comfort in buildings, and therefore help to reduce both light and HVAC energy use. From a health standpoint, artificial lighting tends to suppress melatonin production, thus ensuring increased vigilance and therefore, an improvement in work performance. The harmful effect is occupants cannot be in a serene surrounding. The intake of daylighting can balance this trend by ensuring a space of qualities both in production and in the occupant's welfare. In 1986, in Australia appeared the first innovative device in daylighting: the highly reflective light pipe, commonly known as MLP, for Mirrored Light Pipe. This technology seems to respond to energetic and health criteria. Light pipe allows daylight to be transported and distributed in dark rooms far from traditional openings. They offer the advantage of minimizing light loss while limiting heat transmission.

The behavior of a light pipe can be affected by 3 intrinsic factors and 1 external factor: (i) the collection of daylight (via the collector) (ii) transmission (via the tube), (iii) diffusion (via the diffuser and the area to be illuminated) and (iv) the environment (weather conditions, solar geometry, masks).

Light pipe has attracted considerable interest for nearly 30 years. Thanks to the beneficial effects they provide: reduction in energy consumption, quality of transmitted light, limitation of heat input or, architectural interests. In 1990, Tubular Daylight Guide Systems (TDGS) were judged by Littlefair as the most innovative technology in daylighting (Littlefair, 1990). Many experimental and numerical studies have been carried out to understand the device better. As experience can guide modeling, we conduct a literature review from 1990 to the present by targeting discovery points. The objective is to take stock of experimental knowledge about the light pipe and contribute to the understanding.

1.1 Overall efficiency of the light pipes and energy-saving potential

In 1997, Shao (Shao et al., 1997) presented an experimental study on the performance of light pipe in the United Kingdom during the winter season. They showed that the potential for energy saving is nearly 30 %, and can even increase significantly in the summer period thanks to day length.

Oakley continued the study by highlight the performance of 6 light pipes installed in 3 different areas (store, office, and housing) in Leicestershire, England (Oakley et al., 2000). The results showed that the most effective light pipe is straight, short with a low aspect ratio Ap. The author has noted that if the diameter increases, the device will probably be more efficient. It also highlights the impact of the light pipe on the energy savings achieved. For example, for an office which required lighting level (300 lux), it could be provided whole of the day by the light pipe. Oakley also pointed out that the device affects user satisfaction with the visual comfort that creates a healthier environment.

Based on a coupling of light pipe and artificial lighting (LED), Ji (Ji et al., 2016) studied and improved by simulation, an underground car park at Dalian Nationalities University of China. The author showed that the hybrid lighting system allows an annual energy saving of 60.4 %.

The same year, Malet-Damour (Malet-Damour et al., 2016) proposed to compare the performance of the light pipe to traditional artificial lighting. It was noted that in a clear sky, the light pipe could deliver the equivalent of 10 incandescent bulbs or 5 compact fluorescent bulbs. The light

pipe provides an energy savings of 560 Wh, where artificial lighting is only be used 43% of the time (for a halogen bulb of 70 W).

Other studies have also shown the potential of light pipe (Li et al., 2010; Samuhatananon et al., 2011; Su et al., 2012; Thakkar, 2013; Wu and Li, 2012).

1.2 Parameters related to the illuminated area: colors and dimensions

The wall colors have a notable impact on light distribution due to reflection phenomena. Indeed, the better the reflection coefficient, the higher the number of reflection of incoming light ray (Descartes law), the better light distribution.

This observation allows to adapt the configuration of the room to limit sunspot or dark zone inside, and improved light distribution on the whole workplane. Opposite, dark colors increase the absorption coefficient.

In 1997, Shao (Shao et al., 1997) studied the performance of a light pipe under overcast or clear skies. He showed that the color of the walls of the illuminated area had a substantial effect on the internal illuminance. As a comparative element, he defined the ratio of indoor to global outdoor illuminance. For a white room, this ratio is on average 14 % (under overcast conditions). For black walls and the same weather conditions, this ratio can be as high as 4 %. A ratio of 7 % for white walls versus 2 % for black walls is also announced for clear sky conditions.

This trend is verified in a parametric analysis conducted by Zhang in 2002 (Zhang, 2002) but remains very limited. Indeed, using the DPF model as also described in (Malet-Damour et al., 2016), Zhang specified that its influence does not exceed more than 5 % in the indoor lighting balance.

In 2006, Chella (Chella et al., 2006) proposed a comparative study between the results of numerical and experimental analysis (reduced scale with an artificial sky) for different wall reflectivities (light and dark). The software used for this study were ADELINE 3.0 (International Energy Agency, 2002), ENERGY PLUS (DOE et al., 2016) and ECOTECT (Autodesk, 2008). The authors also considered 2 types of sky: clear and overcast. For a clear sky, Chella showed that indoor reflected component has an impact ranging from 19.4 % to 37.8 % (depending on the position in the place).

As for the geometric aspect, Zhang (Zhang et al., 2002) showed that the performance of the tubular device depends strongly on (i) the Euclidean distance D and (ii) the vertical height of the diffuser H. The author demonstrated that in real-life situations, the diffuser of the light pipe reacts more like a point source than a finite surface. The illumination achieved inside the room is proportional to $(H/D)^{1/3}$ and inversely proportional to D^2 (Bouguer's law).

1.3 Parameters related to the light pipe

In this section, it was noted in the literature that parameters relatives to the light pipe have a notable impact on the quality or quantity of transmitted light. The light pipe could be considered as a black box with several parameters which can affect the light collection, distribution, and quality. Among them (i) the position and inclination of the collector (ii) the presence of dome deflector (iii) the type of surface for the tube straight or elbowed and (iv) the nature of diffuser has been studied since 2002.

1.3.1 Impact of the position and orientation of the collector and its shape

In 2008, Wu (Wu et al., 2008) conducted an experimental analysis of the performance of 1 lateral and 2 zenithal light pipes. Measurements were taken at the same time for each process under real weather conditions (sunny winter day in Beijing, China). If no masks obstruct access to daylight, the results showed that the lateral light pipe offers better results than the zenithal device. A similar study carried out by Duc Hien showed the efficiency of a collector placed on the façade was also (Duc Hien and Chirarattananon, 2009).

In 2012, Kocifaj (Kocifaj et al., 2012) published a study demonstrating the optimal configuration to take advantage of the nominal efficiency of a bent light pipe. It specifies that maximum efficiency is achieved when the collector is oriented towards the solar path and pointed towards the sun. It showed that straight pipe with horizontal collectors is less efficient than a light pipe with a collector inclined towards the sun for clear skies. However, in cloudy skies, the straight pipe captures more of the celestial illuminance.

Sharma (Sharma et al., 2018), with a numerical analysis, studied the optimal geometric shape of the collector. The study showed that a 6° angle of inclination in the lower part of the collector increases the performance of the device.

129 1.3.2 Impact of a deflector in the collector

130 Additional accessories, as light deflector associated with the light collection, increase light
131 capture and significantly improve the efficiency of the light pipe. Azad (Azad and Rakshit, 2018)
132 highlighted the impact of this process on the performance of the light pipe in India. He showed that
133 changing the position of the light deflector can improve the efficiency of the device by more than 2 %.

134 1.3.3 Link between the light spectrum and the colors of the transmitted light

135 The light intensity of a source influences the qualitative perception of ambiances. However, the
136 color of the light delivered has an essential aspect. It is generally assumed that the spectral variations
137 generated by MLP devices do not affect the color of the transmitted light. In 2014, Nilsson (Nilsson et
138 al., 2014) studied and confirmed this hypothesis using spectrophotometer measurements and numerical
139 study for direct and diffuse illuminance. It should be noted that the author ignored the collection and
140 diffusion mechanism. The MLP appears to have achromatic properties.

141 1.3.4 Impact of optical and geometric parameters of the light pipe

142 In 1998, Shao (Shao et al., 1998) studied the performance of light pipe installed in a dozen
143 buildings in the United Kingdom. The performance of the devices was evaluated for 4 types of
144 buildings. The light pipe all had a moderate aspect ratio Ap, and allowed indoor illuminance greater
145 than 450 lux, with a DPF of about 1 %. It is reduced by 0.1 % in the case of a thin and long pipe with
146 an elbow. The author concluded that large diameter pipe should be used as often as possible.

147 A few years later, Ellis (Ellis et al., 2004) showed the influence of the aspect ratio Ap on the
148 transmission coefficient τ_{TDGS} for several light pipe reflectivities. Indeed, in his inter-software
149 comparative study (ENERGY PLUS (DOE et al., 2016) VS. FSEC (McCluney, 2003)), he found that the
150 increase in the aspect ratio causes an exponential drop in transmittance. For example, for a ρ_{LP}
151 reflectivity of 98 %, the transmission coefficient increases from 96 % (Ap=2) to 88 % (Ap=8). The
152 decrease is all the more significant as the reflectivity of the pipe decreases: at ρ_{LP} = 92 %, for an Ap going
153 from 2 to 8, the variation of the transmission coefficient amounts to more than 27 %. Ellis showed that
154 the length of the pipe mainly influences the aspect ratio.

For a given solar altitude and brightness index, the square radius of the tube affects the amount of incoming light. Also, the aspect ratio of the light pipe and the solar altitude influence the transmittance of the device (Zhang et al., 2002).

Maňková's study could support the conclusion of Ellis. The author surveyed MLP straight light pipe (Maňková et al., 2009). He showed the impact of geometric and optical parameters (diameter, length of the pipe, reflectivity) on the light transmission efficiency numerically. Under direct illuminance (clear sky type), as the diameter of the tube increases, the efficiency of the device increases logarithmically. Thus, tube diameter of 20 cm generates a transmission coefficient τ_{TDGS} of 80 % compared to 87.5 % for a pipe of 80 cm. Also, when the reflectivity ρ_{LP} increases, the efficiency increases linearly (τ_{TDGS} = 71.5 % for a tube with a ρ_{LP} of 94 %, against 92 % for a reflectivity of 99 %).

On the other hand, the increase in the length of the pipe leads to an exponential decrease in luminous efficacy. A 1.0 m long tube results in a transmission coefficient τ_{TDGS} of 89 % compared to 58 % for a pipe length of 5.0 m. The observation remained the same for diffuse illuminance (overcast sky), but less pronounced than for direct part. Maňková specified that these results are validated for the type of pipe studied and can evolve according to the reflectivity of the tube.

1.3.5 Impact of elbows of the light pipe

Based on straight and curved pipes (with a single elbow) and for elliptical or rectangular sections, Gupta (Gupta et al., 2001) have numerically studied this problem. He performed a ray-tracing simulation with variations in the radius of curvature. Gupta found that light propagation within the tube is concentrated in the central part for a straight section while it is predominant on the inner periphery for a section with an elbow.

In 2002, Carter (Carter, 2002) set up a study allowing him to compare experimental (in situ and laboratory) and predicted data for the performance of different light pipe configurations. Carter found that an elbow with an angle of 0 to 30 ° results in a loss of efficiency of nearly 20 % (at 30 °, -20 %). Between 30 ° and 90 °, the decrease in efficiency is smaller (about 5 % from 30 ° to 90 °).

The same year, Zhang (Zhang, 2002) showed that the light loss associated with the use of a 30 ° bend was 20 % under overcast conditions. Similarly, Jenkins and Muneer (Jenkins and Muneer, 2004)

conducted a sensitivity analysis on the use of bent light pipe for 30 °, 60 °, and 90 ° inclinations. They found a slight difference in performance between these devices. They deduced an exponential relationship reflecting the losses associated with the transfer within the elbows.

In 2005, to model the performance of a light pipe, Jenkins (Jenkins et al., 2005) continued their study on the impact of elbows. He deduced a ratio of equivalence between the singular light loss caused by an elbow and the linear light loss of a straight pipe. Using experimental measurements on bends from 5 ° to 75 °, Jenkins proposed an equation to calculate the percentage loss for curves at the same angle. The year before, Van Derfolske and Hough (Van Derlofske and Hough, 2004) also studied the impact of elbows on light transmission through the light pipe. They found that a 50 ° bend results in a loss of flux of nearly 50 % while two 25 ° bends result in a loss of only 36 % of the luminous flux. The ratio between the bending and the light loss is not linear.

The CIE report (CIE, 2006) on the efficiency of light pipes recommended the use of a standard 1.0 m long tube and the measurement of incoming and outgoing light fluxes. In this report, the experts used fluorescent lamps mounted on panels incorporating a sphere and 2 pipes connected by an elbow. Several elbow angles were selected for the study (0 °, 30 °, 60 °, 90 °, 2x30 °, and 2x90 °).

Su (Su et al., 2012) conducted an experimental study on commercial light pipes under real climatic conditions contradicting previous results. The experimental results showed that, at equal dimensions, the luminous flux at the exit of the curved light pipes is higher than the straight pipes for clear sky conditions. The results are confirmed numerically. The number of hours of illuminance accumulated between a straight and curved pipe also varies. The bent pipe is more efficient for luminous fluxes greater than 2000 lm. Below this value, the straight and curved pipes are equal.

1.3.6 Impact of the shape of the diffuser and diffusing surface

Zhang (Zhang et al., 2002) tested the impact of the type of diffuser on the evolution of the DPF. To do this, the author experimented with a straight diffuser and a curved diffuser. He noted that the DPF reached with the flat diffuser is higher than that achieved with the curved diffuser.

In 2008, Wu (Wu et al., 2008) experimentally studied 2 types of diffusers: a prismatic diffuser (diamond type) and an translucent diffuser (snow type). Experimental data showed that the light pipe

equipped with the translucent diffuser achieves better performance than the device with the prismatic diffuser.

A study similar to that of Wu was also conducted by Baroncini (Baroncini et al., 2010). He tested 2 types of polycarbonate diffusers, one characterized by a prismatic geometry, the other characterized by a radial geometry, but completely transparent in the center. The conclusions were the same as those of Wu.

Kennedy (Kennedy and O'Rourke, 2015) proposed and tested a new form of vertical light pipe containing lateral openings serving several levels of a building.

1.3.7 Impact on thermal comfort conditions

Williams (Williams and Dorville, 2014) experimentally studied the thermal performance of light pipe in a seminar room located in Beijing, China. The results showed that a significant temperature gradient during the day could increase energy consumption to maintain a temperature of 25 °C. Indeed, in clear sky, the diffuser temperature was 6.68 °C higher than the ambient temperature, and the collector nearly 4.45 °C warmer than the diffuser. At night, the author showed that the light pipe behaves like a thermal bridge because the temperature of the dome is always lower than the diffuser temperature and the room temperature at night.

1.4 Parameters related to the environment of the light pipe

1.4.1 Impact of outdoor illuminance level and seasonality

The behavior of a daylighting device depends naturally on solar radiation. Callow (Callow, 2003), during this thesis, achieved a parametric analysis of the performance of light pipes. His measurements were made in Nottingham and Singapore, and allowed to develop models for evaluating the effectiveness of light pipes. He concluded that the efficiency of the light pipe was not always proportional to the external illuminance.

A few years later, Li (Li et al., 2010) continued the analysis, and experimentally studied the performance of straight light pipes equipped with sensors inside positioned according to different radii of a circle. It showed that the transmittance of the device is not a constant value for a given pipe. It

varies according to the amount of external illuminance. In this case, device efficiency (defining by the ratio between the outgoing and incoming luminous flux) ranged between 0.14 and 0.27.

Two years later, Kocifaj (Kocifaj et al., 2012) confirmed these results and showed the effect of seasonality on the behavior of the light pipe. In summer, the average luminous flux under the light pipe elbowed is only slightly higher than the luminous flux with a straight tube. In spring and autumn, it increases. For temperate climates, the author has also concluded that the devices transmit more light if they are curved.

Based on experimental data, Vasilakopoulou (Vasilakopoulou et al., 2017) analyzed the spatial and temporal variability of indoor lighting using clustering techniques. There is an exponential relationship between average and maximum indoor and outdoor illuminance levels.

1.4.2 Impact of solar altitude, sky brightness index and angle of incidence of the incoming beam

Zhang (Zhang et al., 2002; Zhang and Muneer, 2000) and Carter (Carter, 2002) experimentally studied the impact of solar altitude on the transmittance of the device. This meteorological parameter modifies the number of inter-reflections within the tube. As the solar altitude increases, the number of inter-reflections decreases, resulting in better transmittance. Wu (Wu et al., 2008) considered that solar altitude is the main factor affecting the performance of the light pipe. He concluded that the light distribution in a clear sky is asymmetrical and depends on the position of the sun. Zhang also pointed out that the brightness index kt and solar azimuth can also affect indoor daytime illuminance, depending on the light pipe configuration (confirmed by (Darula et al., 2010)). In the tropics, the luminous efficiency of the light pipes is better due to the predominant high solar altitude and long sunshine duration. On the other hand, in temperate climates, and particularly in winter, these 2 parameters do not make possible to take advantage of the performance of a light pipe, although necessary during this period (Darula et al., 2010).

Hansen (Garcia Hansen et al., 2009) showed that solar altitude impacts the angle of incidence of incoming rays. The light loss in a tube is related to the multitude of reflections that the wave undergoes. Consequently, a light beam with the most significant angle of incidence minimizes the

number of reflections and thus improves the performance of an MLP device. There are 2 solutions to achieve this objective: (i) expand the system components or (ii) improve the collection system. This finding was confirmed by Darula (Darula et al., 2010). Edmonds (Edmonds, 2010) also discussed another aspect of the impact of the angle of incidence of penetrating rays. The variation of this angle has a significant impact on the efficiency of the light pipe that can be related to the angular dependence of the reflectivity on the Fresnel surface (perfect smooth mirror). The trend is verified and confirmed through Swift's study (Swift, 2010). It showed that the transmittance of the light pipe decreases significantly during months when the incidence angles of penetrating rays are low (winter).

Few years later, Vasilakopoulou (Vasilakopoulou et al., 2017) used a statistical approach (clustering analysis) to confirm the existence of a correlation between the overall transmittance of the light pipe, the solar azimuth and the solar altitude in clear sky.

In 2018, Tsang (Tsang et al., 2018) confirmed Edmonds and Swift results by also specifying that light transmission is a monotonous function of solar altitude, except for low angles (winter, beginning, and end of the day).

1.4.3 Dissociate direct and diffuse illuminance

As we have seen in the last section, the type of sky has a notable impact on light distribution. Consequently, it is necessary to decompose the direct (significant in clear sky) and diffuse (major in an overcast sky) illuminance.

In 2009, Mohelnikova (Mohelnikova, 2009) conducted a study on a straight light pipe. It showed that the luminous flux at the diffuser outlet and the distribution of illuminance under the diffuser is uniform and symmetrical when the sky is overcast. In clear skies, this distribution is not directly uniform.

Two years late, Lo Verso (Lo Verso et al., 2011) showed with simulations under SkyVision that it is more accurate to decompose light (direct and diffuse). He justified it by means of an experiment on a Mirrored Light Pipe for 2 types of sky (overcast and clear).

The distinction between clear ad overcast skies can be made by the solar altitude whose the influence in the clear sky is notable. Oh (Oh et al., 2013) showed using a diagram "Candela power

distribution curve - CDC" that the light distribution of the light pipe is directly related to the solar altitude. He concludes that the light pipe uses all the components of daylight (diffuse and direct), but that direct light influences the light distribution.

1.4.4 Impact of condensation and dust

Dust and condensation that may form in light pipes can affect their performance. Wu (Wu et al., 2012) experimentally studied this link by measuring the transmitted luminous flux under 3 different conditions (cleanliness, dust, and condensation) and for clear and overcast sky conditions. The results showed that dust has a more significant impact on the performance of the device than condensation. In clear skies, condensation reduces transmission by 6.37 % compared to 15.31 % for dust. In overcast conditions, the cleanliness of the dome results in a reduction of 24.05 % compared to 17.2 % for condensation.

1.5 Variability of all parameters

In 1995, Swift and Smith (Swift and Smith, 1995) studied the links between the design and material parameters for a circular MLP device. They calculated the transmission coefficient precisely by using an optical analysis of the propagation of light rays along a tube. The authors derived an equation involving the reflectivity of the pipe, aspect ratio, and angle of incidence of incoming rays. This study clearly showed that the performance of the light pipe depends on many parameters, which can themselves vary considerably.

1.6 Originality of the paper

Table 1 summarizes all the studies identified from 1990 to 2019 and classified by theme.

All the studies reviewed were conducted under temperate or continental climatic conditions in the Northern Hemisphere. These experimental conditions made it possible to evaluate the behavior of the light pipes for nominal illuminance levels of around 100 Klux in clear sky. This paper presents the only experimental data in the southern hemisphere (different solar path) and for extreme sunlight conditions. In these climatic conditions, we come to refute, confirm, and bring a new perspective on the behavior of the Mirrored Light Pipe. We demonstrated the close link between the type of sky, the solar path, the indoor light distribution, and the lighting levels achieved. We also showed that the energy-

316 saving potential generated by the light pipe in tropical environments and associated with different colors
317 of the area to be illuminated. We also proposed an experimental analysis of the interest of a solar
318 concentrator placed in the dome of the device. We have also evaluated the impact on indoor lighting of
319 a mandatory device in cyclonic areas of the globe: the anticyclonic sub-dome.
320 All these results offer an additional step forward in the understanding of the behavior of the
321 Mirrored Tubular Daylight Guide Systems and contribute to the enhancement of this technology.

322 **2. Materials and methods**

323 As seen in the previous review, it is necessary to study the light pipe environments to
324 understand their behavior. Reunion Island is very particular due to his intense solar irradiation, that is
325 why, we choose to set up experimentation to verify and validate observations from the literature.

326 **2.1 Experiment set-up**

327 The measurements are carried out on an experimental cell, called LGI (Miranville, 2002), and
328 located in Saint-Pierre, Reunion Island. The arrangement of the empirical support has been made
329 considering the sun's path and promoting an orientation without obstacles to the wind. The LGI is
330 oriented North/North-West (9° N). Representing a small building of 9 m², it consists of vertical opaque
331 walls made of composite panels, a glass door (north facade), a blind (hidden) and a horizontal ceiling.
332 The dimensions are described in Figure 1. The sloping roof (20 °) is made of corrugated night blue sheet
333 metal. A Mirrored Light Pipe (SOLATUBE®) has been installed in the roof plane and is curved to
334 ensure the horizontality of the diffuser. The walls of the device have an internal reflection coefficient of
335 99.7 %. An impact study revealed that the far-mask effect was negligible.

336 **2.2 Measurement and data acquisition**

337 Daylight measurements are collected from AHLBORN type devices with their central data
338 acquisition systems. These devices are synchronized with each other and record at the time step of a
339 minute. The indoor illuminance is measured from 9 luxmeters, positioned as shown in Figure 2 so that
340 each sensor is located on a circle of different diameter whose center is A0. The workplane is fixed at 10
341 cm from the ground. The external luxmeters are used to measure global and diffuse illuminance (Figure
342 3). The measurement of diffuse illuminance is ensured by the shadow ring designed in the laboratory,

called SHADECO. The procedure of conception and validation of this device is described in (Malet-Damour et al., 2018).

The test cell was adapted to correspond to each experimental scenario. By measuring indoor and outdoor illuminances, it was tried to confirmed or refuted the findings reviews about the influence of the type of sky on light distribution in the southern hemisphere. That is why the wall colors have been colored to black (deleted the reflection part of diffusing light). Also, by changing wall colors, it was possible to understand the impact of this parameter (the reflection coefficient) on the light level. Other scenarios were conducted to quantify the effects of 2 devices used to improve light collection (changing the position of a reflector in the dome) or to protect the light pipe (anticyclonic sub-dome).

All experimental scenarios were synthesized in Table 2.

3. Results and discussion

3.1 Solar deposit of climate study

We carry out a brief climatic analysis of the environment in which the light pipe is positioned. The objective is to understand the solar potential of the city of Saint Pierre, Reunion Island. We seek to discern the annual evolution of the global outdoor illuminance measured with an external luxmeter.

Figure 4 highlights a significant seasonality in global illuminance corresponding substantially to the seasons present in Reunion Island. The southern summer extends from November to April. This is the period when the solar deposit is most abundant. The days are longer, with a maximum illuminance frequently between 150 Klux and 200 Klux (in clear sky), and the beginning and end of the day close to 50 to 75 Klux.

The southern winter, from May to October, is the period when the maximum illuminance is around 100 to 125 Klux. The days are shorter. Mornings and ends of the days provide less than 75 Klux of light. The trend changes as early as August when the days recover from hours of sunshine.

Seasonality does not seem to be properly related to the lighting needs. Indeed, a system using daylight within a building will offer significant efficiency from September to April, and less for the rest of the year.

3.2 Impact of sky type on light distribution

The objective was to see the impact of the type of sky on the light distribution within the room (see Table 2, scenario N°1). All the inner walls of the cell are covered with a black wallpaper (reflection coefficient close to 0.05). The objective is to eliminate factors that can influence the light distribution within the room. The part of the internal reflections being negligible, the light pipe is then the only light source in the room (Figure 5).

The day of September 23, 2014 presents a clear sky with a maximum global outdoor illuminance of 120 Klux. The contribution of the celestial vault is less than 17 Klux (see Figure 6). These conditions are typical of sunny conditions for a clear day in winter on Reunion Island.

Under the diffuser (A0), we notice that the maximum values for indoor illuminance are not at solar midday (marked by a vertical blue dotted line). When the global outdoor illuminance reaches its maximum during the day, the light pipe does not generate an illuminance that can be considered as a maximum in the area. Indeed, we can see that at this same time, the A1 sensor has illuminance values close to 600 lux. The other sensors do not seem to show any particular event.

Overall, if we refer to the hourly evolution of the illuminance for each instrument, we see between 1 and 2 unsynchronized peaks of illuminance appear during the day. These events are localized. Their evolution is linked to time and space. We assume that these are "sunspots" depending on the position of the Sun.

The distribution of illuminance on the ground within the room is presented for different hours (Figure 7). This mode of representation is commonly used in lighting thanks to the ease with which a light distribution can be imaged on a work surface.

We select representative hours, where the indoor illuminance is important enough to allow us to observe a phenomenon. At 9:00 am, the average illuminance is about 150 lux, and the light distribution appears to be angularly uniform. In the following hours, the distribution no longer seems to follow Lambert's law because the maximum illuminances change position over time. At 11:00 am in particular, the maximum illuminance is located southeast while the Sun is oriented northeast. When the Sun is in the axis of the light pipe (due North), the distribution seems to refocus around the central point (under the diffuser in A0). The following hour we notice an opposite position to the 11:00 am

event: the maximum illuminance is located South-West while the Sun is located in the North-West axis. The following hours resemble the first hours of the day by not marking any particular orientation in the distribution of indoor illuminance.

In all likelihood, the position of the Sun impacts the light distribution, and more precisely, direct illuminance does not follow the law of logical diffusion because the source moves during the day.

Visually, we can confirm these results. Figure 8 shows solar bands marked by more intense illuminance. If a light band is positioned on one of the sensors, it will detect high illuminance without the phenomenon being visible through the other instruments. Unlike Baroncini's findings (Baroncini et al., 2010), these pictures clearly shows that the diffuser does not allow a distribution according to Lambert's law. Maybe these solar bands are not high enough to be visible under lower solar irradiation.

To conclude, direct lighting is not distributed rigorously throughout the room. It is localized and generates light bands with high illuminance levels. In a global approach, the phenomenon observed being localized, it would be necessary to consider the global impact of these "sunspots".

We are now looking to visualize the photometric phenomena for an overcast day (November 30, 2014). As can be seen in Figure 9, the global outdoor illuminance follows the trend of diffuse part. A maximum illuminance is recorded at 10:00 am and may correspond to a partial clearing of the clouds. Otherwise, the outdoor global and diffuse illuminances are around 50 Klux between 9:30 am and 2:30 pm.

As the direct outdoor illuminance is close to zero, we notice that the time evolution at each measurement point is similar (Figure 9). To justify this observation, we focus on an event (marked by a red dotted vertical line). This event could correspond to the passage of a denser cloud. It is reflected inside the cell at the same time. We find that the further away the measurement point is far from the diffuser, the more the illuminance decreases proportionally. This behavior suggests a distribution from an orthotropic light source.

Overall, we notice that in overcast skies, the daily evolution of indoor and outdoor illuminances correctly follows the same progression.

Using the same methodology as for clear sky, we plot the evolution of light distribution within the room for different hours (Figure 10). In the configuration of an overcast sky, the illuminance levels achieved are much lower than those obtained in clear sky. The average deviation under the diffuser is close to 200 lux.

During the hours of the day, the illuminance distribution does not change. At 9:00 am, the illuminance in the center of the room increases (200 lux), then decreases in the following hours to increase again at 1:00 pm. Overall, we confirm the observation made in the previous curves: the luminance increases, but remains stable according to the direction of emission: the illuminance distribution follows Lambert's law.

In conclusion, the light pipe can be considered as a black box that reflects the input/output load, with one inversion. In this way, the diffusion within the room can be uniform in an overcast sky, and directional in a clear sky in extreme solar irradiation environments.

3.3 Impact of the color of the area to be illuminated: evaluation of the energy-saving potential

This study consists of varying the colors of the interior walls of the area to be illuminated and understanding their impact on indoor lighting and artificial lighting autonomy (see Table 2, scenarios N°1 to 5). We will use the average reflection coefficient to compare the different situations. This parameter is calculated retain proportion to the surfaces of each color. We assume that the reflection coefficients of the walls are constant and known: (i) white wall reflection coefficient: (ii) black wall reflection coefficient: (iii) grey wall reflection coefficient: .

In this way, Table 2 shows the values of this parameter according to the experimental scenarios.

To take into account the impact of this parameter on the energy autonomy of the room, we consider the room as an office which required a minimum lighting level of 200 lux (according to the European standard EN 12 464-1). That's why we calculate the percentage of time the lighting level is higher than needed.

Our reference will be scenario N°5 (5 white walls and 1 grey wall). We will compare events from one year to another. The reference case data cover the years 2013 and 2014, while the other scenarios

were conducted from 2014 to 2015. By comparing the same dates for different years, we are assured that the solar path is theoretically similar. Thus, the solar altitude and azimuth can deviate from the influential parameters. We will use an hourly ratio of the average indoor illuminance (average of the hourly illuminance recorded by the indoor luxmeters) to the outdoor global illuminance. This ratio gives a general trend in the time evolution of illuminance in terms of usefulness, which excludes the impact of direct part on the light distribution within the room. We select days with similar outdoor global illuminance profiles from one year to the next.

Comparison of scenarios N°1 and 5

The days of November 21, 2013 and November 21, 2014 are clear sky days (Figure 11). The hourly profile of outdoor global illuminance from one year to another is similar with a maximum illuminance of around 131 Klux. The patterns of the ratios are related to a close coefficient: the part with the highest reflection coefficient has the highest rate. Indeed, by increasing the average reflection coefficient from 0.05 to 0.699, we increase the average indoor illuminance by 47 % on average. When the cell has its black walls, the light pipe allows autonomy in lighting nearly 3 % of the time compared to 37 % for the case study N°5. This means that 3 % of the time we are above 200 lux, the minimum required level. As a result, the artificial top-up is inevitable 97 % of the time (in clear sky) compared to 63 % for a room with white walls.

Comparison of scenarios 2 and 5

March 16, 2015 is a clear day. The same day of 2014 is partially covered (Figure 12). These two days have the most comparable profiles of the measurement period of study case N°2. The maximum outdoor global illuminance is about 120 Klux. The pattern of the ratios of the studied cases is similar. The increase in the average reflection coefficient from 0.162 to 0.699 increases the average useful indoor illuminance by 42 %. The scenario N°2 allows being autonomous almost 10 % of the time compared to 32 % for the case N°5. For an area with 5 black walls and 1 white wall, artificial lighting is unavoidable 90 % of the time (in clear sky) compared to 68 % for a room with white walls.

Comparison of scenarios 3 and 5

The days of March 24, 2014 and March 24, 2015 are clear-sky days with a similar time profile for global outdoor illuminance (Figure 13). The maximum illuminance is about 121 Klux. With one factor aside, the ratios are similar. By increasing the average reflection coefficient from 0.274 to 0.699, we increase the average indoor illuminance by 36 % on average and thus be energy self-sufficient 17.5 % of the time compared to 39.8 % in case N°5. The use of artificial lighting is unavoidable 82.5 % of the time (in clear sky) compared to 60.2 % for a room with white walls.

Comparison of scenarios 4 and 5

The days of April 3, 2014 and April 3, 2015 are also clear sky days with a similar time profile for global outdoor illuminance (Figure 14). The maximum illuminance is about 113 Klux. Both days have a ratio profile identical to a factor. By increasing the average reflection coefficient from 0.385 to 0.699, we increase the average indoor illuminance by 35 % on average. It reduces the artificial lighting level to 82.3 % of the time (in clear sky) compared to 60.8 % for a room with white walls.

Synthesis

Overall, we find that the reflection coefficient of the walls has a considerable impact on the average illuminance within the area. The more we have an area with clear walls, the more we will increase the useful average illuminance. This is due to the absorption coefficient of the black walls, considerably limiting the internally reflected illuminance.

This observation can be illustrated in Figure 15. By moving from a room with black walls to a room with white walls, we can double the level of indoor illuminance and thus limit the use of an additional artificial lighting system. This observation makes it possible to complete what the literature had revealed to us in the previous section (Chella et al., 2006; Shao et al., 1997; Zhang, 2002).

3.4 Impact of the position of a dome deflector

In the southern hemisphere, the northern orientation is preferred to increase the performance of solar devices. At the summer solstice (December 21), the Sun rises in the East/South-East and sets in the West/South-West. At the winter solstice (June 21), the Sun rises in the northeast and sets in the northwest. A deflector device, placed in the dome, maximizes the collection of solar rays.

We wanted to evaluate the impact of deflector positions on the amount of light inside the area to be illuminated for the configuration of the light pipe studied (curved tube with the collector in the plane of the roof). That is why, measurements were made by positioning the deflector in different orientations (North, South, East, and West), as described in Table 2, with the scenarios N°6 to 9). Figure 16 shows the different positions tested and the solar-path of the study city (Saint-Pierre, Réunion). "North" orientation means that the deflector is facing south (back to the north).

Before identifying the most optimized orientation of the deflector to increase the collection of solar rays, we seek to evaluate the impact of this device on the supply of daylight within the area to be illuminated. We compare the effect of the deflector positioned to the South (facing the North, orientation recommended by the manufacturer, scenario N°7) for a clear sky when the walls of the room are black. The deflector-free measurements were obtained in December 2014. Measurements with deflector are collected during February 2015, at the rate of one week of collection per orientation. To rule out the impact of the solar-path, we will use the ratio between the useful average indoor and global outdoor illuminance, averaged over the measurement period.

We can see that the deflector increases the amount of daylight (Figure 17). However, the device does not significantly improve the performance of the light pipe.

Concerning the impact of the deflector orientation, and concerning the experimental data, we find for each a clear measurement period, intermediate and cloudy sky days. Since the solar path is not the same from one day to the next, and therefore from one configuration to another, we determine the impact of the deflector position from an average ratio. This ratio is the ratio between the indoor and global outdoor average illuminance during the period. With measurements in diffuse illuminance, and neglecting the part of the reflected illuminance (no mask to consider), we obtain direct illuminance (from the subtraction of diffuse from global illuminance). We apply an impact ratio to the previously calculated average one by determining the proportion of diffuse and direct impact on indoor illuminance. Then, we can learn, by orientation, two essential pieces of information (i) the relationship between the position of the deflector and the overall efficiency (ii) the relationship between the effectiveness of the deflector, its location and the type of illuminance (direct or diffuse).

Figure 18 confirms that positioning the deflector in the South (deflector facing North, scenario N°7) increases the efficiency of the light pipe. The figures are still close for the North position (facing South, scenario N°6) this being probably because the collector is inclined in the plane of the roof. Moreover, at this time of year (see Figure 16, red line of the solar path), the Sun passes from East to West with an almost similar part of the day when the collector sees the Sun in the South and North. The East (scenario N°9) and West (scenario N°8) positions are optimal for capturing morning or late afternoon light rays, respectively.

By looking at the differentiation of diffuse and direct illuminance, we can see that (i) direct part has a more significant impact on the level of indoor illuminance for a deflector positioned in the South (scenario N°7), (ii) diffuse part is predominant in the supply of light for a deflector in the North. For the East and West orientations, diffuse and direct illuminances have a similar impact.

We deduce that it is preferable to orient the deflector to the North or South (in the case where the collector is inclined to the North) for the Southern Hemisphere. This position can also change during the year, depending on the weather conditions. Tropical summer is marked by more cloudy days (predominant diffuse illuminance), the deflector could be placed in the North, and conversely in winter (mostly clear sky).

3.5 Tropical arrangement: impact of the anticyclonic sub-dome

During a tropical cyclone, several extreme phenomena can damage or even destroy a structure (wind gusts, torrential rain, floods, debris carried by wind or rivers, landslides, etc.). In general, an anticyclonic construction is designed to withstand the direct effects of wind, airborne debris, and rain. It is, therefore, a question of designing and building constructions with a sufficient level to ensure the three essential functions: mechanical resistance, shelter from wind and rain. That is why it is necessary to protect the fragile areas of a building. The technological difficulty is to establish a compromise between resistance and tightness without hindering the primary function. The light pipe, because of its position on the building represents a point of fragility. There is an anticyclonic sub-dome to compensate for shocks related to flying debris. Reunion Island is one of the areas where this is necessary.

555 This case study (see Table 2, scenario N°10) is specific to geographical areas subject to
556 anticyclonic provisions. The sub-dome is installed on the light pipe, as shown in Figure 19. We are
557 trying to evaluate the impact of this sub-dome on the overall performance of the light pipe.

558 As before, we will base our analysis on the ratio between the average indoor and outdoor
559 illuminance. This will allow comparing days whose solar geometry will not be the same. We will examine
560 the average daily ratio for configurations with and without the anticyclonic sub-dome for a test cell with
561 black walls. We only use clear sky days to assess the maximum impact of the sub-dome.

562 We find that the anticyclonic sub-dome has an impact on the transmission factor of the light
563 pipe τ_{TDGS} (Table 3). This additive element reduces light transmission by an average of 9.2 % ± 3 %.
564 While it may be negligible for indoor illuminance achieved in clear sky, it will be essential to take into
565 account its contribution in the overcast sky.

566 **Conclusions and perspectives**

567 A literature review permitted to identify and to class each parameter, which could have an impact
568 on light pipe performance and light distribution inside the illuminated area. It was noted that
569 geometric, optic or climatic parameters relatives to (i) illuminated area (ii) light pipe (iii) environment of
570 the device, have a notable impact on indoor light distribution and light level. All the studies reviewed
571 were conducted under temperate or continental climatic conditions in the Northern Hemisphere.

572 This paper presents the only experimental data in the southern hemisphere (different solar path)
573 and for extreme sunlight conditions. It permitted to understand and apprehend the behavior of the
574 light pipe under the intensive climatic condition of Reunion Island. We found that the light
575 distribution within the room was strongly related to the type of sky. In cloudy skies, the diffuser behaves
576 like an orthotropic source whose diffusion follows a Lambertian law. Indeed, the light pipe acts as a
577 black box. The profile of the indoor illuminance is similar to the profile of the outdoor. In a clear sky,
578 the observation is no longer valid. The indoor lighting becomes directional, linked to the position of the
579 Sun. Lambert's law is no longer valid.

This work also allowed to test other experimental configurations such as the variation of the colors of the illuminated area. We noted that the increase in the average reflection coefficient could result in a significant increase in the average indoor illuminance. Energy autonomy is the most revealing parameter of the study, showing that switching from a dark to a bright room avoided the use of an artificial light source no less than 37 % of the time.

It was also studied the optimal position of a reflector placed in the dome to increase the collection of solar rays. Reunion Island is located in the southern hemisphere at latitude 21 °S. In this region of the globe, and given the sun path, it is common to orient solar devices to the North. The study confirmed that our collector with deflector, inclined in the roof plane (20 °), is the most efficient when facing North. A lack of orientation could lead to a drop of nearly 20 % in the light transmission of the light pipe.

Considering the location and cyclonic concerns of Reunion Island, it was tried to evaluate the impact of an anticyclonic sub-dome placed under the primary collector. Experimental results concluded that it reduces 9.2 % of the average transmission of the light pipe.

This paper was intended to contribute to the experimental photometric study of Mirrored Light Pipes. A thermal experimental study has starting to understand the impact of the light pipe on indoor ambient conditions and the user thermal comfort in the tropical climate.

References

Autodesk, 2008. ECOTECT ANALYSIS.

Azad, A.S., Rakshit, D., 2018. Experimental Study of Tubular Light Pipe System: Influence of Light Reflector on Its Performance, in: Sayigh, A. (Ed.), Transition Towards 100% Renewable Energy: Selected Papers from the World Renewable Energy Congress WREC 2017, Innovative Renewable Energy. Springer International Publishing, Cham, pp. 21–30. https://doi.org/10.1007/978-3-319-69844-1_3

Baroncini, C., Boccia, O., Chella, F., Zazzini, P., 2010. Experimental analysis on a 1:2 scale model of the double light pipe, an innovative technological device for daylight transmission. Sol. Energy 84, 296–307. https://doi.org/10.1016/j.solener.2009.11.011

607 Callow, B.J., 2003. Daylighting Using Tubular Light Guide Systems. University of Nottingham.
608 Carter, D.J., 2002. The measured and predicted performance of passive solar light pipe systems. Light.
609 Res. Technol. 34, 39–51. https://doi.org/10.1191/1365782802li029oa
610 Chella, F., Zazzini, P., Carta, G., 2006. Compared numerical and reduced scale experimental analysis on
611 light pipes performances ., in: Proceedings of the 5 Th International Conference on Sustainable
612 Energy Technologies {SET}. pp. 1–6.
613 CIE, 2006. Tubular daylight guidance systems. Vienna. Comm. Int. l'Eclairage 173:2006, 3–38.
614 Darula, S., Kocifaj, M., Kittler, R., Kundracik, F., 2010. Illumination of interior spaces by bended
615 hollow light guides: Application of the theoretical light propagation method. Sol. Energy 84,
616 2112–2119. https://doi.org/10.1016/j.solener.2010.09.003
617 DOE, BTO, NREL, 2016. Energy Plus.
618 Duc Hien, V., Chirarattananon, S., 2009. An experimental study of a facade mounted light pipe. Light.
619 Res. Technol. 41, 123–139. https://doi.org/10.1177/1477153508096167
620 Edmonds, I., 2010. Transmission of mirror light pipes with triangular, rectangular, rhombic and
621 hexagonal cross section. Sol. Energy 84, 928–938. https://doi.org/10.1016/j.solener.2010.03.001
622 Ellis, P.G., Strand, R.K., Baumgartner, K.T., 2004. Simulation of Tubular Daylighting Devices and
623 Daylighting Shelves in Energyplus, in: Conference, I.-U.N. (Ed.), SimBuild 2004. Boulder,
624 Colorado, pp. 1–8.
625 Garcia Hansen, V., Edmonds, I., Bell, J.M., 2009. Improving daylighting performance of mirrored light
626 pipes: Passive vs. active collection systems, in: PLEA 2009 - Architecture Energy and the
627 Occupant's Perspective: Proceedings of the 26th International Conference on Passive and Low
628 Energy Architecture. Quebec City, Canada.
629 Gupta, A., Lee, J., Koshel, R.J., 2001. Design of efficient LightPipes for illumination by an analytical
630 approach. Appl. Opt. 40, 3640–3648.
631 International Energy Agency, I., 2002. ADELINE.
632 Jenkins, D., Muneer, T., 2004. Light-pipe prediction methods. Appl. Energy 79, 77–86.
633 https://doi.org/10.1016/j.apenergy.2003.11.003

Jenkins, D., Muneer, T., Kubie, J., 2005. A design tool for predicting the performances of light pipes. Energy Build. 37, 485–492. https://doi.org/10.1016/j.enbuild.2004.09.014

Ji, S., Cao, G., Zhang, J., Yu, F., Li, D., Yu, J., 2016. Lighting design of underground parking with tubular daylighting devices and LEDs. Optik (Stuttg). 127, 1213–1216. https://doi.org/10.1016/j.ijleo.2015.10.189

Kennedy, D.M., O'Rourke, F., 2015. Experimental analysis of a scaled, multi-aperture, light-pipe, daylighting system. Sol. Energy 122, 181–190. https://doi.org/10.1016/j.solener.2015.08.013

Kocifaj, M., Kundracik, F., Darula, S., Kittler, R., 2012. Availability of luminous flux below a bended light-pipe: Design modelling under optimal daylight conditions. Sol. Energy 86, 2753–2761. https://doi.org/10.1016/j.solener.2012.06.017

Li, D.H.W., Tsang, E.K.W., Cheung, K.L., Tam, C.O., 2010. An analysis of light-pipe system via full-scale measurements. Appl. Energy 87, 799–805. https://doi.org/10.1016/j.apenergy.2009.09.008

Littlefair, P. j., 1990. Review Paper: Innovative daylighting: Review of systems and evaluation methods. Light. Res. Technol. 22, 1–17. https://doi.org/10.1177/096032719002200101

Lo Verso, V.R.M., Pellegrino, A., Serra, V., 2011. Light transmission efficiency of daylight guidance systems: An assessment approach based on simulations and measurements in a sun/sky simulator. Sol. Energy 85, 2789–2801. https://doi.org/10.1016/j.solener.2011.08.017

Malet-Damour, B., Boyer, H., Guichard, S., Miranville, F., 2017. Performance Testing of Light Pipes in Real Weather Conditions for a Confrontation with Hemera, in: Journal of Clean Energy Technologies. Hong Kong - Chine, pp. 73–76. https://doi.org/10.18178/jocet.2017.5.1.347

Malet-Damour, B., Guichard, S., Bigot, D., Boyer, H., 2016. Study of tubular daylight guide systems in buildings: Experimentation, modelling and validation. Energy Build. 129, 308–321. https://doi.org/10.1016/j.enbuild.2016.08.019

Malet-Damour, B., Guichard, S., Jean, A.P., Miranville, F., Boyer, H., 2018. SHADECO: A low-cost shadow-ring for diffuse measures: State of the art, principles, design and application. Renew. Energy 117, 71–84. https://doi.org/https://doi.org/10.1016/j.renene.2017.09.083

Maňková, L., Hraška, J., Janák, M., 2009. Simplified Determination of Indoor Daylight Illumination By

Light Pipes. Slovak J. Civ. Eng. 4, 22–30.

McCluney, R., 2003. Rating of Tubular Daylighting Devices for Visible Transmittance and Solar Heat Gain - Final Report. Cocoa, Florida.

Miranville, F., 2002. Contribution à l'étude des parois complexes en physique du bâtiment : modélisation, expérimentation et validation expérimental de toitures complexes incluant des produits minces réfléchissants en climat tropical humide. La Réunion.

Mohelnikova, J., 2009. Tubular light guide evaluation. Build. Environ. 44, 2193–2200. https://doi.org/10.1016/j.buildenv.2009.03.015

Nilsson, A.M., Jonsson, J.C., Roos, A., 2014. Spectrophotometric measurements and ray tracing simulations of mirror light pipes to evaluate the color of the transmitted light. Sol. Energy Mater. Sol. Cells 124, 172–179. https://doi.org/10.1016/j.solmat.2014.01.049

Oakley, G., Riffat, S.B., Shao, L., 2000. Daylight performance of lightpipes. Sol. Energy 69, 89–98. https://doi.org/10.1016/S0038-092X(00)00049-9

Oh, S.J., Chun, W., Riffat, S.B., Jeon, Y. Il, Dutton, S., Han, H.J., 2013. Computational analysis on the enhancement of daylight penetration into dimly lit spaces: Light tube vs. fiber optic dish concentrator. Build. Environ. 59, 261–274. https://doi.org/10.1016/j.buildenv.2012.08.025

Samuhatananon, S., Chirarattananon, S., Chirarattananon, S., Chirarattananon, P., 2011. An experimental and analytical study of transmission of daylight through circular light pipes. LEUKOS - J. Illum. Eng. Soc. North Am. 7, 203–219. https://doi.org/10.1080/15502724.2011.10732147

Shao, L., Elmualim, A.A., Yohannes, I., 1998. Mirror lightpipes : Daylighting performance in real buildings. Light. Res. Technol. 30, 37–44. https://doi.org/10.1177/096032719803000106

Shao, L., Riffat, S.B., Icks, W.H., Yohanne, I.S., 1997. A Study of Performance of Light Pipes Under Cloudy and Sunny Conditions in the UK. Right Light 1, 155–159.

Sharma, L., Ali, S.F., Rakshit, D., 2018. Performance evaluation of a top lighting light-pipe in buildings and estimating energy saving potential. Energy Build. 179, 57–72. https://doi.org/10.1016/j.enbuild.2018.09.022

Su, Y., Khan, N., Riffat, S.B., Gareth, O., 2012. Comparative monitoring and data regression of various sized commercial lightpipes. Energy Build. 50, 308–314. https://doi.org/10.1016/j.enbuild.2012.03.053

Swift, P.D., 2010. Splayed mirror light pipes. Sol. Energy 84, 160–165. https://doi.org/10.1016/j.solener.2009.10.008

Swift, P.D., Smith, G.B., 1995. Cylindrical mirror light pipes. Sol. Energy Mater. Sol. Cells 36, 159–168. https://doi.org/10.1016/0927-0248(94)00172-3

Thakkar, V., 2013. Experimental study of Tubular Skylight and comparison with Artificial Lighting of standard ratings. Int. J. Enhanc. Res. Sci. Technol. Eng., 6 2, 4–9.

Tsang, E.K.W., Kocifaj, M., Li, D.H.W., Kundracik, F., Mohelníková, J., 2018. Straight light pipes' daylighting: A case study for different climatic zones. Sol. Energy 170, 56–63. https://doi.org/10.1016/j.solener.2018.05.042

Van Derlofske, J.F., Hough, T.A., 2004. Analytical model of flux propagation in light-pipe systems. Opt. Eng. 43, 1503. https://doi.org/10.1117/1.1753272

Vasilakopoulou, K., Kolokotsa, D., Santamouris, M., Kousis, I., Asproulias, H., Giannarakis, I., 2017. Analysis of the experimental performance of light pipes. Energy Build. 151, 242–249. https://doi.org/10.1016/j.enbuild.2017.06.061

Williams, D., Dorville, J.-F., 2014. Investigating the Thermal and the Lighting Performance of Light Pipes for Sunny and Cloudy Conditions in Insular Tropical Climate. Electr. Eng. 2, 221–227. https://doi.org/10.17265/2328-2223/2014.05

Wu, Y., Jin, R., Li, D., Zhang, W., Ma, C., 2008. Experimental investigation of top lighting and side lighting solar light pipes under sunny conditions in winter in Beijing, in: Wang, A., Liao, Y., Song, A., Ishii, Y., Fan, X. (Eds.), 2008 International Conference on Optical Instruments and Technology: Advanced Sensor Technologies and Applications. p. 71571O. https://doi.org/10.1117/12.811992

Wu, Y., Li, H., 2012. Experimental study on performance of top lighting solar light pipes in the meeting room in winter in Beijing. Appl. Mech. Mater. 178–181, 29–32.

https://doi.org/10.4028/www.scientific.net/AMM.178-181.29

Wu, Y.P., Wang, X.D., Chen, Z.G., Zhang, C.Y., 2012. Experimental Study on the Influence of Daylighting Performance of Solar Light Pipes by Dusts and Condensation, in: Sustainable Development of Urban Environment and Building Material, Advanced Materials Research. Trans Tech Publications Ltd, pp. 1096–1099. https://doi.org/10.4028/www.scientific.net/AMR.374-377.1096

Zhang, X., 2002. Daylighting Performance of Tubular Solar Light Pipes: Measurement, Modelling and Validation. Napier University of Edinburgh.

Zhang, X., Muneer, T., 2000. Mathematical model for the performance of light pipes. Light. Res. Technol. 32, 141–146. https://doi.org/10.1177/096032710003200306

Zhang, X., Muneer, T., Kubie, J., 2002. A design guide for performance assessment of solar light-pipes. Light. Res. Technol. 34, 149–168. https://doi.org/10.1191/1365782802li041oa

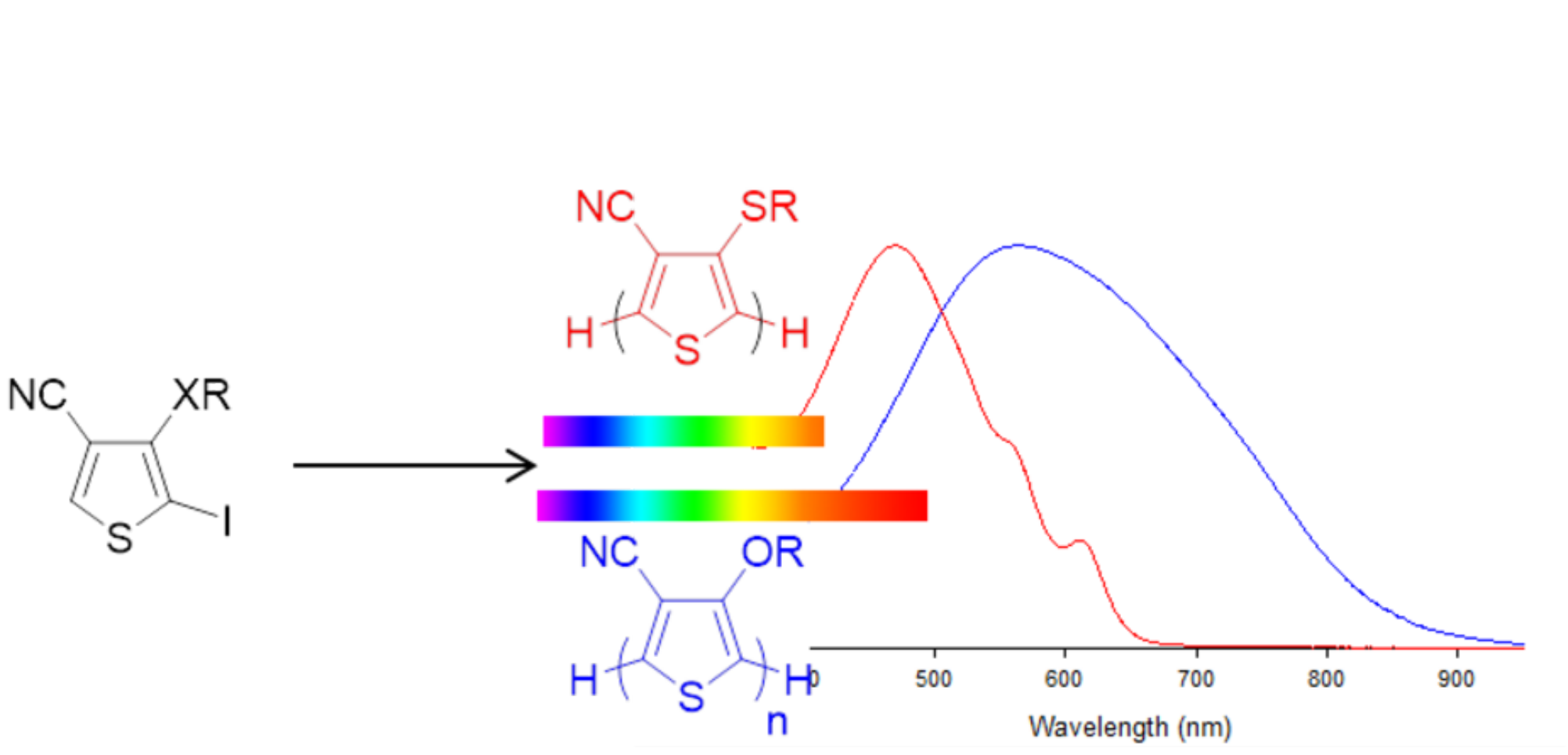
NC
XR
S
I
NC
SR
H
S
H
NC
OR
H
S
H
n
500
600
700
800
900
Wavelength (nm)